The Hong Kong Polytechnic University

Department of Health Technology and Informatics

DEVELOPMENT OF COMPUTATIONAL MODEL FOR TOTAL KNEE ARTHROPLASTY DESIGN

WONG WAI CHI, DUO

A thesis submitted in partial fulfilment of the requirements for

the Degree of Master of Philosophy

November 2009

CERTIFICATE OF ORIGINALITY

I hereby declare that this thesis is my own work and that, to the best of my knowledge and belief, it reproduces no material previously published or written, nor material that has been accepted for the award of any other degree or diploma, except where due acknowledgement has been made in the text.

_____ (Signed)

WONG WAI CHI (Name of Student)

Abstract of thesis entitled

Development of Computational Model for Total Knee Arthroplasty

Submitted by

Wong Wai Chi, Duo

for the degree of Master of Philosophy in Biomedical Engineering

at The Hong Kong Polytechnic University

in November 2009

Total Knee Arthroplasty is a common option to treat knee pain and restore knee function for osteoarthritis patients, though failure is inevitable. Implant manufacturers often focus on mechanical performance of implant, such as contact area, stress and fatigue, and consider individual response of knee geometry less, whilst evaluation of design on subject performance could be useful, but require years of continuous assessment and sometimes unfeasible. Computational methods provide an efficient and objective approach to investigate the parametric effects of loading, surgical deviation and design variations in a well-controlled environment, with both consideration of implant and knee components. Understanding these effects and their mechanisms can aid engineers and physicians to design better implants and establish optimal surgical protocols.

The 3D geometry of knee was constructed and segmented from Magnetic Resonance (MR) images, whereas the geometry of implant was acquired from scan of digitizer. The model were assembled and simulated with surgical procedures and processed with finite element (FE) analysis. Parametric study was then carried out to evaluate different effects, such as load and bone strength on different flexion angle, and gait conditions. Two kinds of parametric studies have been done in this study. The first study aimed to evaluate the contact stress of the tibial insert at different load, flexion angle and gait conditions. The results could be verified and compared with existing experiments and finite element results. The second study focused on the investigation of effect of variation of the bone stiffness on the stress of trabecular femur, and aimed to study the mechanism of periprosthetic fracture upon reduction of bone stiffness.

In the study of contact stress of tibial insert, the FE prediction showed that the contact stress ranged from about 23MPa to about 25MPa. This result was comparable to that of existing literatures, ranged from about 17MPa to about 27MPa. Although the predicted stress exceeded the allowable stress 10MPa of

UHMPWE for the tibial insert, it did not reach the yield strength of UHMWPE. In the gait study of tibial insert, the contact stress formed two peaks at about 16% and 45% gait cycle, with contact stress about 53MPa and about 29MPa, respectively. The latter stress was comparable to existing literatures that peak stress occurred at 45-55% of gait. The former stress peak may be due to over-constrain on specific implant kinematics by input boundary conditions of gait.

In the study of bone strength on trabecular femur, the predicted stress was concentrated on the apex of screw-hole, posterior supra-condylar region and anterior flange, consistent with clinical observation of peri-prosthetic fracture. The maximum predicted stress increased by about 3.87% and 2.94% at 5-degree and 60-degree flexion, respectively when the bone strength was reduced by half. Although the increase of the predicted stress was relatively small, the reduction in bone strength resulted in reduction in bone sustainability. By comparing the predicted stress and yielding stress upon bone strength reduction, it was shown that the risk of stress yielding or micro-fracture at the trabecular layer was likely even at lower flexion angle. Since the maximum predicted stress shifted to the anterior flange region at higher flexion angle, the design of implant anterior flange contributed to improve the stress distribution anteriorly especially at higher flexion angles. This computational model could provide an efficient platform to investigate the change of stress distribution and magnitude on bone-implant upon sensitivity of different parameters. This model could aid physicians and designers to design better implants and surgical protocols.

ACKNOWLEDGEMENTS

My university life at The Hong Kong Polytechnic University started at 2002. It has been about 7 years since I admitted in this university. I changed departments from the Mechanical Department to the Department of Health Technology and Informatics (HTI) currently. I found my interest and target of academy in this period of time. Professor Zhang Ming was the first professor that I met when I was taking an interview in the HTI department, and now he is my supervisor of this research. I would like to take this opportunity to express my deep gratitude to Professor Zhang Ming for the support and guidelines, not only for my research study, but starting from giving the opportunity for me to join this department. Professor Zhang Ming has provided indispensable encouragement and patience to my study, as well as invaluable suggestions to my research content and written work. I would also like to thank my co-supervisor Professor Qin Ling from the Chinese University of Hong Kong for providing clinical information and suggestions on my study. I would also like to express my sincerely thanks to my co-supervisor Dr. Chi Fai Cheung, from the Department of Industrial and Systems Engineering of The Hong Kong Polytechnic University for his guidance and technical support in the engineering aspects in the fabrication and measurement of the implants.

Secondly, I would like to thank Professor Arthur F.T. Mak, Professor Iris Benzie, Professor Huang Wei and Professor Mo Yang, for giving me comments to optimize my research directions and methodologies.

Thirdly, I would also like to thank Dr. Jason Cheung and Dr. Lawrence Yu for giving me technical support of the finite element analysis and all other software. I may not be taken up those sophisticated software by myself within this short period of time without them. I would like to thank Miss Lesie Ho from the Department of Industrial Systems and Engineering, for the collaboration in the manufacturing part of the project.

I would like to acknowledge all of my other fellow colleagues whose supported my research, Miss Christina Lee, Mr. Li Ho Yip, Mr. Man Hok Sum for helping me in the rehabilitation clinic, Miss Angela Huang, Miss Cong Yan, Miss Crystal Liu, Dr. He Gong, Dr. Hongquan Zhang, Miss Lizhen Wang, Dr. Tina Yan for contribution of my study, especially on the content of kinematics.

I would also express my sincere thanks to all the research staff and students in the department for their warm support. Special thanks are also expressed to my friends and family, for their support, especially upon my time of depression.

Finally, I would like to acknowledge the Research Grant Council of Hong Kong, Department of Health Technology and Informatics and the Innovation and Technology

Commission (ITC) (GHP/052/06) of the Government of the Hong Kong Special Administration Region for the financial support of my study in the project.

PUBLICATIONS ARISING FROM THE THESIS

Conference Proceedings

Wong WC, Zhang M, Cheung CF and Qin L, Development of knee finite element model for implant design. The BME 2008 Hong Kong Biomedical Engineering International Conference, Hong Kong, 23-25 Oct 2008.

Duo Wai-Chi Wong, Jason Tak-Man Cheung, Chi-Fai Cheung, Ling Qin and Ming Zhang, Finite element analysis on the effect of bone strength on periprosthetic fracture. XXII Congress of the International Society of Biomechanics, Cape Town, South Africa, 5-9 Jul 2009.

Duo Wai-Chi Wong, Chi-Fai Cheung, Ling Qin and Ming Zhang, sensitivity of trabecular modulus to tibial stress shielding, The World Association for Chinese Biomedical Engineers (WACBE) World Congress on Bioengineering 2009, Hong Kong. 26-29 Jul 2009

Book Chapters

M. Zhang, W.C. Wong and C.F. Cheung. Overview of Development of Orthopedic Implant. In: Technical Guidebook for Supporting Design, Fabrication and Measurement of Orthopedic Implant for Biomedical Applications. Edited by C.F. Cheung, W.B. Lee, M. Zhang and S. To., pp. 11-23., The Hong Kong Polytechnic University. ISBN: 978-962-367-690-8.

W.C. Wong, M. Zhang and C.F. Cheung. Modeling and Analysis for Supporting Design of Orthopedic Implant In: Technical Guidebook for Supporting Design, Fabrication and Measurement of Orthopedic Implant for Biomedical Applications. Edited by C.F. Cheung, W.B. Lee, M. Zhang and S. To., pp. 24-57. The Hong Kong Polytechnic University. ISBN: 978-962-367-690-8.

Journal Paper

Duo Wai-Chi Wong, Ming Zhang, Chi-Fai Cheung and Ling Qin, Identifying Risk of Periprosthetic Fracture: A Sensitivity Study, (in preparation)

TABLE OF CONTENTS

LIST OF FIGURES

LIST OF TABLES

CHAPTER I INTRODUCTION

1.1 Total Knee Replacement (TKR) – Treatment for the Painful Knee

The TKR was firstly reported in late 1950s. The design and fit of the implant have improved in the past 10 years and is now believed to be safe and effective in treating pain and restoring function (Rankin et al., 2004). Osteoarthritis (OA) is the most common indication for knee replacement. Other indications are rheumatoid arthritis (RA), juvenile RA, osteo-necrosis and other inflammatory arthritis. TKR is an elective procedure to suggested candidates with radiographic evidences of joint damage and persistent pain (Rankin et al., 2004). After the surgery, functional outcome would generally be improved across the disability spectrum. About 85% of the patients are satisfied with the result of surgery, rapid and substantial alleviating of pain and improving health-related quality of life (Rankin et al., 2004).

1.2 Osteoarthritis – Prevalence

In 2000, the World Health Organizaion (WHO) reviewed and summarized existing prevalence studies of OA globally. The prevalence data is summarized in **Fig. I-1**. It was estimated that approximately 10% of population would have symptomatic OA by the age of 60. The studies were not consistent in comparing the prevalence rate of developing and developed countries. However, gender, ethnic and geographical differences were shown. Females were more affected after age of 55. The review showed that African American was more liable to OA than Caucasian American (Murray et al., 2001).

In 2001, The review of Green showed that 80% of the population would have radiographic evidences of OA by the age of 65, of which 60% of them would be symptomatic. It was approximated that 300,000 TKR surgeries would be taken place for end-stage arthritis patients in the United States (Rankin et al., 2004). In 2005, the demand of replacement surgeries were grown by 70% in five years. In view of the growing demand of implant, obesity epidemic and need for revision surgery, the total number of replacement by 2030 would be expected to be nearly 4.5 million in the US (Natalia et al., 2008).

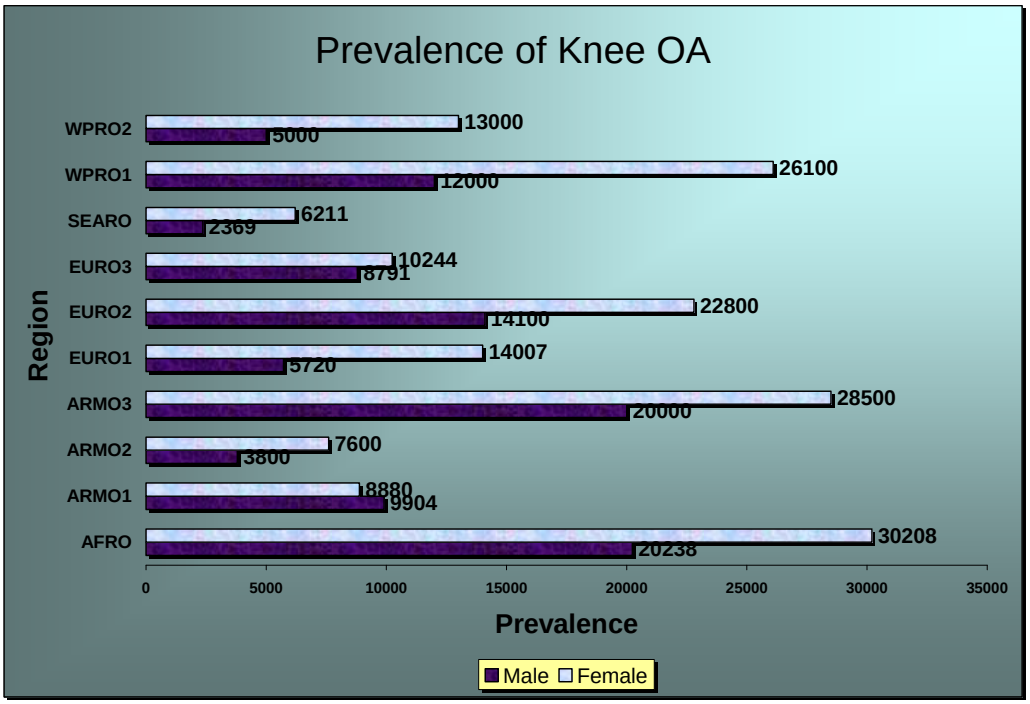

Table I-1 The prevalence of osteoarthritis in different regions (Murray et al., 2001)

Ref.	Population	Year	Diagnostic Criteria
Solomon et al. (1975)	Rural Tswana population of Phokeng, South Africa (AFRO)	-	Clinical Assessment Kellgren & Lawrence Criteria
Davis et al. (1988)	Probability samples of the US civilian, non-institutionalised population (AMRO1)	1971-75	Radiographs Kellgren & Lawrence Criteria
NHANES I	Probability sampes of US civicilian, non-institutionalised population (AMRO2)	1971-75	Radiographs Kellgren & Lawrence Criteria
Bremner et al. (1968)	Lawrence Tavern, Jamaica (AMRO3)	-	Radiographs Kellgren & Lawrence Criteria
Carmona (2000)	Spanish population, continential and islanders (EURO1)	1998-99	Clinical and ACR Criteria
Valkenburg (1980)	Zoetermeer, Holland (EURO2)	1975-78	Radiographs
Tzonchev (1968)	Sofia, Bulgaria (EURO3)	-	Radiographs
Gibson et al. (1996)	Karachi, Pakistan (SEARO)	-	Clinical Assessment
Tamaki & Koga (1994)	Inhabitants of Matsudai Town, Japan (WPRO1)	1979 and 1986	Radiographs
Hoaglund (1973)	Hospitalised Hong Kong Chinese at Queen Elizabeth Hospital (WPRO2)	1967	Kellgren & Lawrence Criteria

OA incidence and prevalence cases are increasing with age. The incident rate is appeared to be higher at older age. The improvement of life expectancy but lacking of joint replacement becomes a problem to some developing countries. Besides age, gender was another important attributes as OA was more common in females (**Fig. I-2**). Some other factors, such as family history, increase the risk of OA. Diabetes mellitus, osteoporous, obesity, history of trauma, smoking, habits, as well as wearing high-heeled shoe, are associated with OA. Occupations requiring repeated knee bending, such as miners (Kellgren & Lawrence, 1952), dock workers (Partridge & Duthie, 1968), and farmers (Croft et al., 1992) presented a higher opportunity in OA.

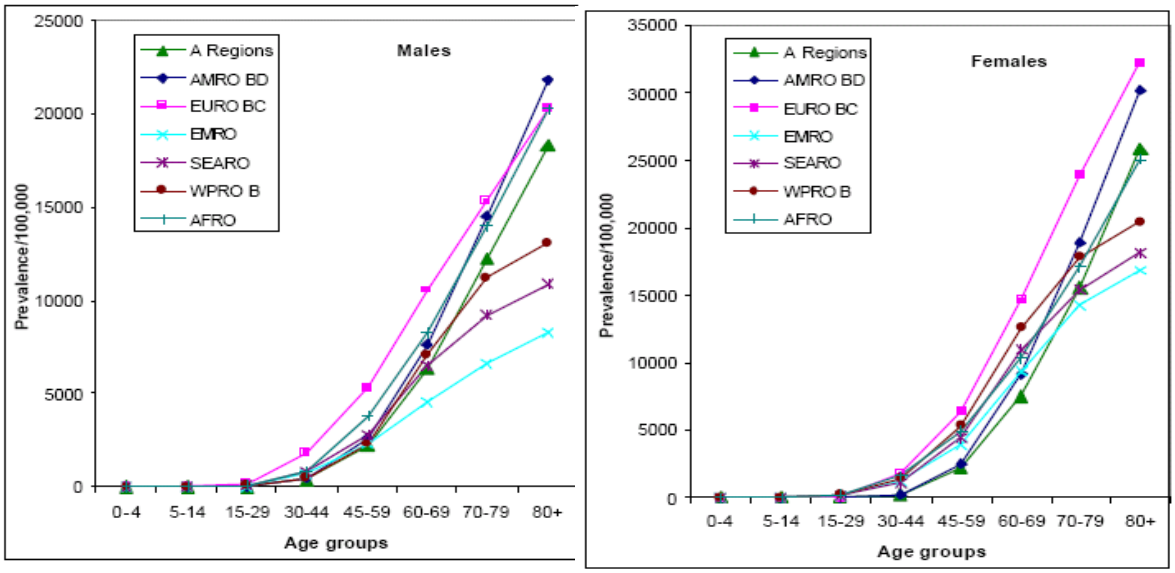

Fig. I-1 Knee OA prevalence rates with age group, sex and region (Deborah et al., 2000).

1.3 Osteoarthritis – The Global Burden

One of the methods in describing Global Burden of Disease (GBD) was mentioned in the WHO paper (Murray et al., 2001). The GBD is estimated by the total of Years of Life Lost (YLL), Years of Lost due to Disability (YLD) and Disability- Adjusted Life Years (DALYs). The GBD of OA in 2000 (Deborah et al., 2000) was compared with the GBD in 1990 (Murray & Lopez, 1997) in **Table I-2**.

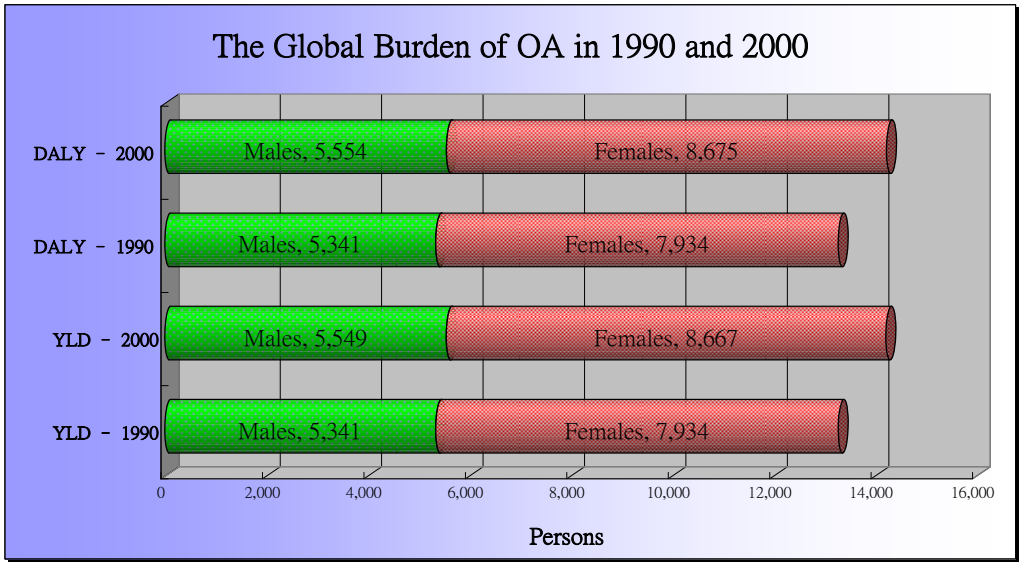

Fig. I-2 Global total YLD, YLL and DALY of OA estimated in 1990 and 2000 (Deborah et al., 2000; Murray & Lopez, 1997).

Table I-2 Global total YLD, YLL and DALY of OA estimated in 1990 and 2000 (Deborah et al., 2000; Murray & Lopez, 1997).

	Males	**Females**	**Persons**
YLD – 1990	5,341	7,934	13,275
YLD – 2000	5,549	8,667	14,216
YLL – 1990	-	-	-
YLL – 2000	5	8	13
DALY – 1990	5,341	7,934	13,275
DALY – 2000	5,554	8,675	14,230

From **Table I-2**, the above table, it was found that the prevalence of male to female was about 4 to 6. The trend of GBD was increasing in terms of YLD and DALY. The proportion of YLD and DALY increase was roughly similar, about 4% and 9% respectively, 7% overall. With the aforementioned causes and risk, the GBD of OA is expected to increase.

In the United States, the hospitalization cost of the implant operation is high, and is ranked one of the top ten common operations. In 2004, knee arthroplasty procedures costed 488,000 hospital stays, with average 3.9 days and $13,200 per admission (Natalia et al., 2008). The cost of payers upon knee arthroplasty was more than $5 billions in 2006 and accounted for more than 50% of reimbursement (Natalia et al., 2008). The high demand of knee implant was reflected by the net sales of Zimmer, one of the largest manufacturers of implants. The company doubled the sales by 2007 in four years (U.S. Securities and Exchange Commission, 2005) with an increase of selling price of 132% since 1996 (Orthopedic Network News, 2008). The huge bills for knee replacement would cause financial problems to the hospitals system, insurances and public welfare.

1.4 Yet Painful Implant

With the high prevalence and heavy global burden imposed by OA, the demand of implant is high. In Hong Kong, it was shown that 7.7% of OA patients required a knee replacement and 3.7% required a hip replacement (Woo et al., 2004). With the aging population, the number of people using joint replacement is expected to increase.

Despite the advancement of implant technology, failure is still inevitable. This fact was supported by the rate of revision TKR treatment (Rankin et al., 2004). The main reasons of implant failure are loosening and wear. Aseptic and mechanical loosening would result in joint instability and exaggerate the problem of wear. The wearing of articular bearing surface could result in osteolysis and infection, and eventually failure. RA patients, which implemented with steroid-therapy, would have a higher chance of peri-prosthetic fracture because of alerted bone density, of which has similar pathology to osteoporotic patients. All these reasons could result in implant failure, that may require revision surgery.

The limited lifespan of implant material contributes to the inevitable failure of the implant. In fact, malalignment, mismatch, poor kinematics and geometry design of implant and surgical procedure would affect the stress distribution between the implant components and between the implant-bone interface that would speed up the wear and tear, and loosening process (Thomas, 1991). While some of the design features, such as stress distribution and stress shielding, range of motion and stability, need to be traded off, the optimal features remain a challenge to implant designers.

Rankin et al. (2004) summarized factors influencing TKR performances as factors related to surgeons' experiences, technical factors and prosthetic designs. It was suggested that surgeons' experience and technique were the most influential factors for better outcome. Hospitals or surgeons that perform more operations per year had a fewer complications rate; Technical factors such as alignment of the prosthesis would affect the wear rate, chance of osteolysis and loosening. While computer navigation is believed to improve alignment and tracking, the technology is expensive and the efficiency is unclear; the prosthetic design nowadays has converged to similar features and different designs showed roughly similar merits. Yet, lacking of practicability and efficiency, custom-made implants are not popularized in the industry, patients are using pre-fabricated implants and

the outcome of mismatch contributing from fitting standardized implants to subject-specific geometry is still on research platform.

1.5 Mismatch

Since mismatch contributes from poor design, the problem is now one of the design problems that implant manufacturers are eager to tackle, of which racial and gender disparities are of clear evidence. Hitt et al. (2003) studied the variation of Medial-Lateral (ML) /Anterior-Posterior (AP) dimension between gender (**Fig. I-3**) and dimension of several implant systems (**Fig. I-4**). Ho et al. (2006) underwent research to evaluate five prosthetic systems : Duracon and Scopio (Stryker Howmedics Osteonics), NexGen (zimmer, Warsaw, indiana), PFC Sigma (Deputy – Johnson and Johnson, Warsaw, Indiana) and Uknee (United Ortho Co., Taiwan) , and showed that they had different overall AP and ML dimension that may be suitable to different populations. Since there were few distinct designs for Asian populations, the author commented that many of these systems that probably designed for Caucasians patients may not be suitable for Chinese patients.

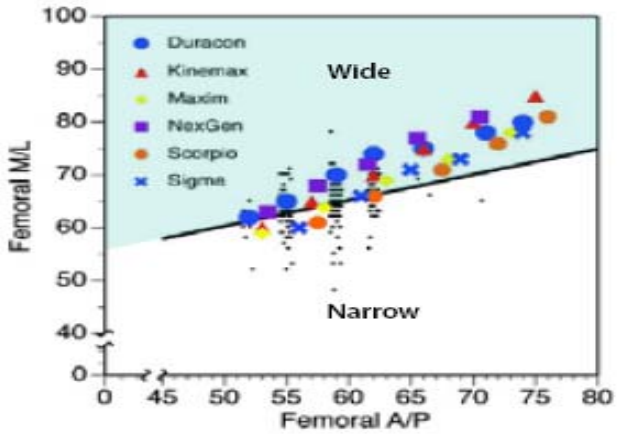

Fig. I-3 The ML and AP difference with respect to gender. (Hitt et al., 2003)

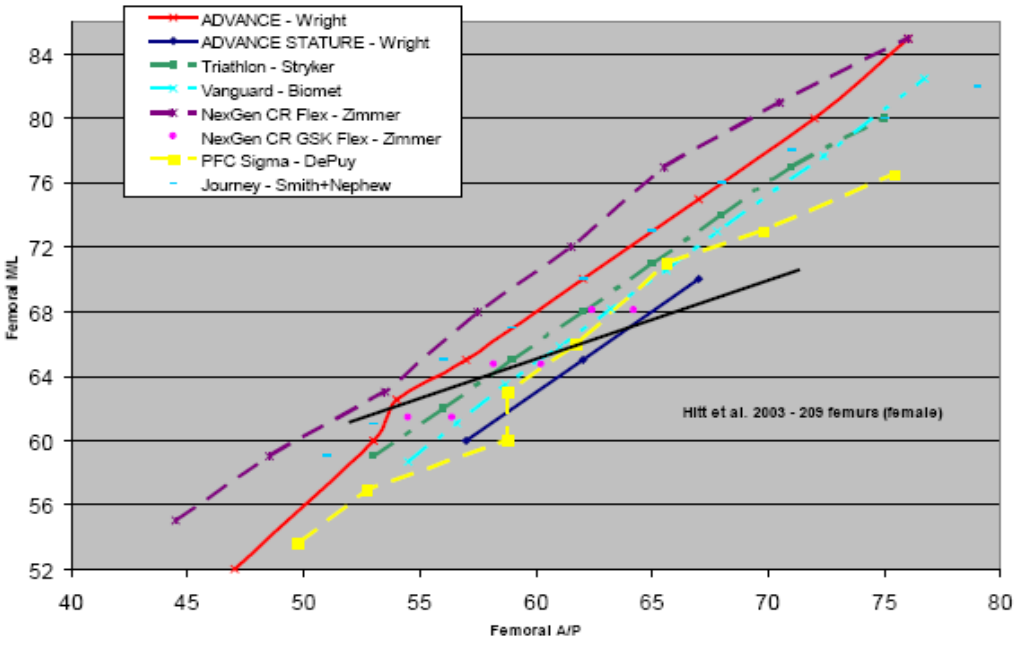

Fig. I-4 Dimensions of several implant systems (Hitt et al., 2003)

Customization is always ideal yet viable. The outcome of mismatch, such as geometry, alignment and functional requirements that deteriorate the implant longevity and failure, is unclear. While the most important feature of implant was pain-relief and the most sensitive factor of implant success was surgeons' experiences (Rankin et al., 2004), the cost-effectiveness of further optimizing implant designs for individual subject's response remains doubt.

As experiment and evaluation of knee implants could take about 5-10 years clinically, computational platform to evaluate implant design could reduce the time of design cycle. The platform could facilitate better understanding on the design factors that influence implant performance, not only empirical comparison on mismatch parameters.

In the long run, a semi-customization approach could be adopted in the industry. A mass production on different sizes could be preliminary produced. With the patient's subject-specific knee geometry, computational platform could determine the optimization and adjustment approach on the implant. Finally, the fine adjustment could be realized by numerical and precision polishing and machining, whereas customization can be compromised with manufacturability.

1.6 Objectives of this Study

TKA is a common treatment option to osteoarthritis knee. However, experiments of TKA requires years of continuous assessment and sometimes unfeasible. Computational method provides an efficient and objective approach to investigate the parametric effects in a well-controlled environment.

The objective of this project was to establish a TKA computational platform. The platform started with the reconstruction of knee and implant model by clinical imaging and reverse engineering technique. The surgical alignment and resection were simulated in the platform. The assembly was then exported to FEA software to carry out stress analysis. At last, parametric study was carried out to verify the capability of the platform. In this study, the parametric study was focused on studying the contact stress of the tibial insert, von Mises stress of trabecular tibia, as well as the bone-implant interface. These studies were compared with existing literatures and clinical findings.

1.7 Outline of the Dissertation

After the introductory chapter, chapter II would start with introduction of functional anatomy of knee joint. The chapter would be followed by reviewing existing knee implants and explain their design features and development over years. A detailed review of existing finite element analysis would then be discussed.

The process of finite element method in this study would be introduced in chapter III. The chapter begins with an overall workflow of the method. The geometry reconstruction of the knee and implant model would be then be discussed. The material properties, load and boundary conditions would be mentioned in the section of development of finite element model, followed by the method of validation. The direction of parametric study would be described at the end of this chapter.

The results of the study are presented in Chapter IV. The first three sections would report the predicted results of the FE parametric analyses, based on varying compressive load, trabecular stiffness and flexion angle. The last section would present an overall FE results on a quasi-static simulation of gait.

Chapter V presents a discussion of the results and findings, the dicussion is divided into four sections based on the direction of parametric study. The first

section would focus on the contact pressure of tibial component. The results of this section would compare with existing finite element results for verifications. In the second section, the bone-implant interface is discussed to explain the mechanism of periprosthetic fracture. Von Mises stress, maximum principal shear and strain would be a reference on the risk of fracture. The stress transfer behavior of the bone-implant interface would be discussed in the third section. The fourth section would be focused on preliminary results of validation. Limitations on finite element analysis and this study would be discussed afterwards.

Chapter VI provides a conclusion of the project and some suggestions for possible future development.

CHAPTER II LITERATURE REVIEW

2.1Functional Anatomy of Knee Joint

2.1.1 Knee Anatomy

Knee joint is a synovial joint comprising of distal femur, proximal tibial and patella, of which the interface between the patella and femoral trochlea forms the patello-femoral joint. The medial and lateral femoral condylar together with the respective articular surfaces of the tibial plateau are named as the medial and lateral tibio-femoral joint (**Fig. II-1**).

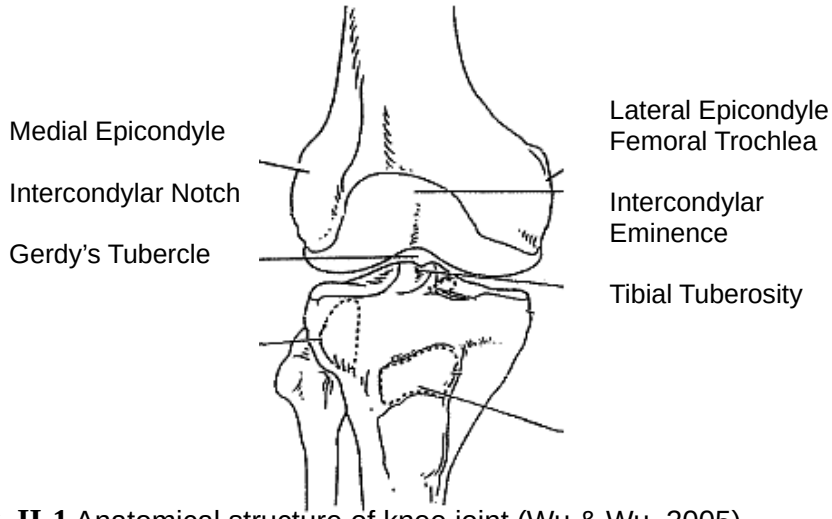

Fig. II-1 Anatomical structure of knee joint (Wu & Wu, 2005)

Patella is the largest sesamoid bone in human body. It forms the extensor apparatus with the tendon of the quadriceps femoris muscles and patella tendon. The thickness of patella is about 20-30 mm; the cartilage layer could be up to 5 mm thick. Three-quarter of posterior patella is the joint articular surface. Another one-quarter area is the insertion point of patella tendon, beyond the joint articular surface.

The anterior side of distal femur is named as trochlea. It divides the femur into medial and lateral portion, and the division line is extended to the intercondylar notch. The intercondylar notch further extends and divides the distal femur into the medial and lateral epicondyles. From sagittal view, the curvature of lateral epicondyle is larger and more protruding, whereas the medial epicondyle is more posteriorly extended (**Fig. II-2**).

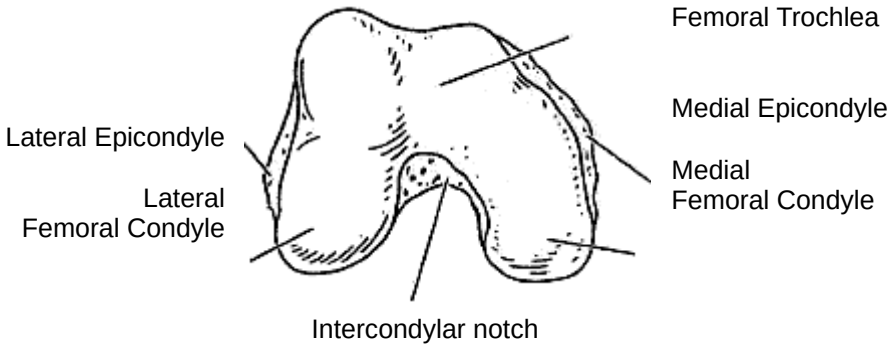

Fig. II-2 Bony structure of distal femur (Wu & Wu, 2005)

The level of tibial plateau is not horizontal. It stands certain degree of posterior sloping higher anteriorly. In the centre of tibial plateau, the meniscus and cruciate ligament are attached nearby the tibial intercondylar eminence. The anterior one-third of lateral tibia joint surface is a gradual rising concave structure, whereas the posterior two-third is a gradual falling concave structure; the medial joint surface is in bowl-concave shape. Thus, the convex articular structure of distal femur could fit with the tibial plateau. The matching of geometry could allow knee flexion and extension to be performed. The rotation of knee flexion/extension is based on instaneous axis of rotation (**Fig. II-3**), mechanically similar to an incongruent or modified hinge joint. Normal range of knee motion has about 135 degrees of flexion and 5-10 degrees of hyper-extension. The flexion and extension motion is a combination of sliding and gliding, and coupled with rotation, abduction and adduction.

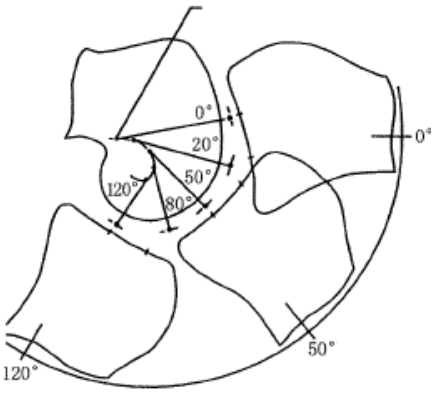

Fig. II-3 Instaneous center of rotation of knee flexion (Wu & Wu, 2005)

Menisci have a triangular shape in cross section. It consists of collagen-fibre structure, with collagen bundles in circumferential arrangement and embedded fibres in radial direction. The pattern could enhance load absorption and structural integrity. Menisci have a superior surface in contact with the femoral condyles and an inferior surface resting on the tibial plateau. The medial meniscus is attached

to the posterior intercondylar fossa. The anterior and posterior opening of menisci is named as anterior and posterior horns, of which attached to the tibia. The anterior horn of the lateral meniscus is attached to the intercondylar fossa, anterior to the lateral tibial tubercle, whereas the posterior horn is attached to the intercondylar fossa, posterior to the lateral tubercle (**Fig. II-4**).

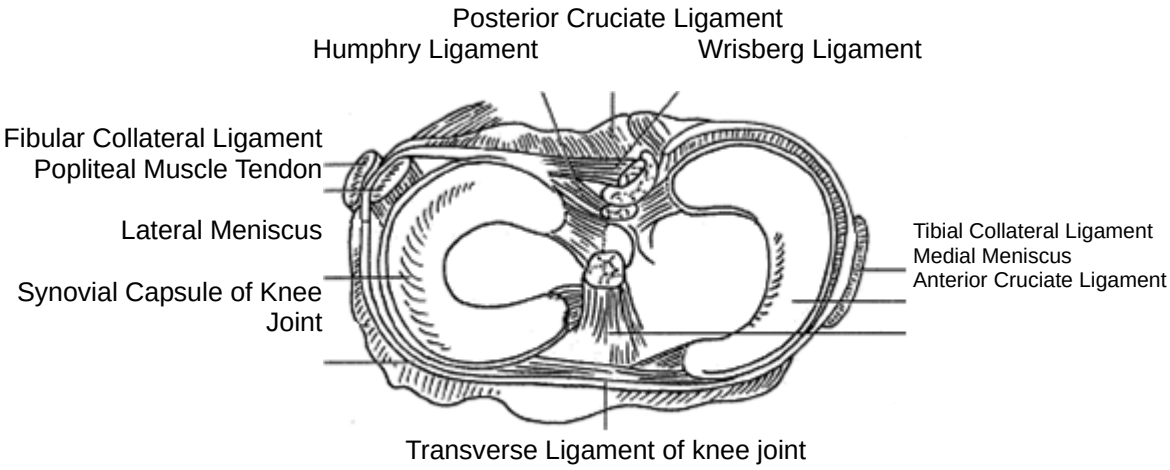

Fig. II-4 Superior view of tibial plateau (Wu & Wu, 2005)

Anterior and posterior cruciate ligament (ACL and PCL) is a strong ligamentous structure in maintaining knee joint stability (**Fig. II-5**). ACL becomes taut while extension (**Fig. II-6**A) and release in flexion (**Fig. II-6**B). It prevents femur from dislocate posteriorly, tibia from dislocate anteriorly, knee hyperextension and over-rotation. PCL becomes taut while flexion (**Fig. II-6**C). It prevents femur from dislocate anteriorly, tibia from dislocate posteriorly and knee over-flexion. ACL starts from the intercondylar eminence, adjacent to the anterior horn of lateral meniscus. It runs laterally, superiorly and posteriorly to connect the medial side of lateral femoral condyle. PCL starts from the posterior intercondylar area of tibia. It runs medially, superiorly and anteriorly to the medial femoral condyle.

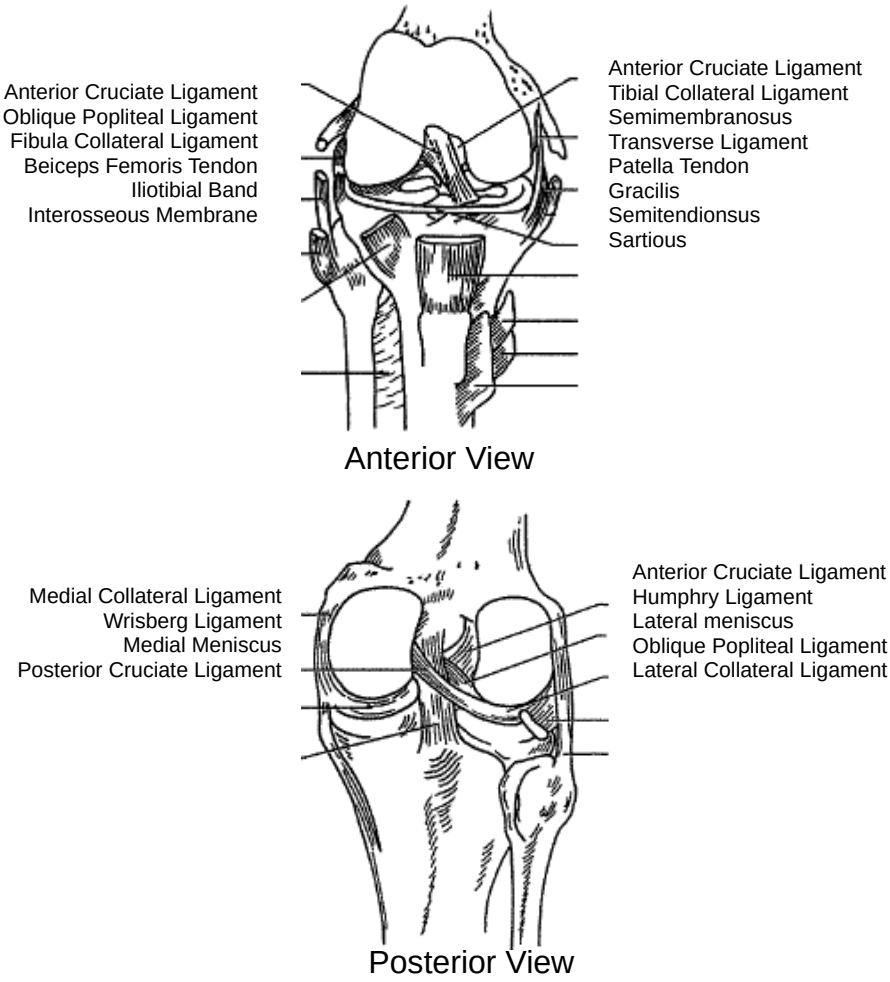

Fig. II-5 Anterior view and posterior view of cruciate ligaments in knee joint (Wu & Wu, 2005)

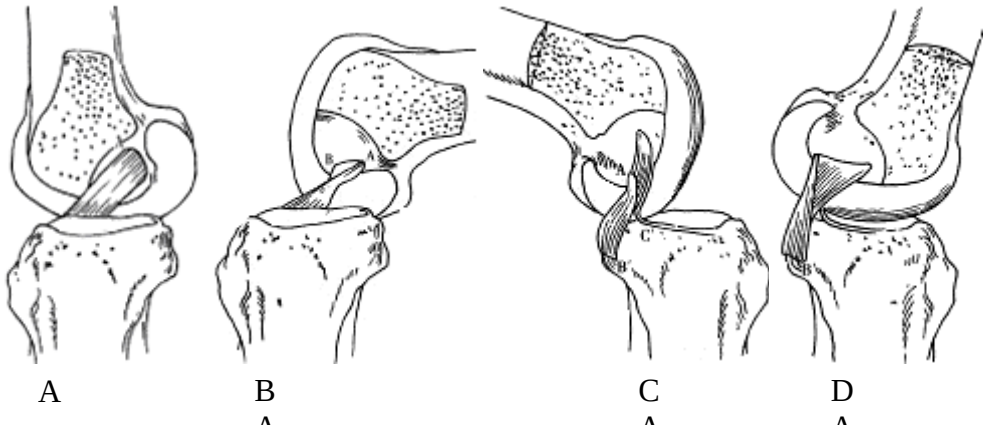

Fig. II-6 Cruciate ligaments in knee flexion and extension (Wu & Wu, 2005).
A. ACL release at extension; **B**. ACL taut at flexion
C. PCL release at flexion; **D**. PCL taut at extension

2.1.2 Anatomical Features in Joint Replacement

2.1.2.1 Knee Alignment

In anatomical posture, the femur head center, knee joint center and ankle joint center are collinear, forming the mechanical axis of lower extremity. The transverse axis of knee joint is parallel to ground level. The anatomical axis of femur shaft forms about 6-degree varus angle with the mechanical axis of knee joint. This valgus angle is different individually and could be related to the femoral anteversion angle and femur neck length. In balanced standing, the joint line of tibial plateau is not parallel to ground level and form about 3 degrees of valgus angle. The valgus angle results in asymmetrical kinematics of knee joint, that cause common medial compartment knee OA.

In planning implant alignment, it is suggested to ignore the knee valgus angle and focus on constructing simple mechanical axis of knee joint. Since the valgus/varus and Q-angle of knee is altered, the joint axis could not be easily approximated by knee joint center in pathological condition. The mechanical axis of knee joint can be measured and constructed by assessment on the residual bones. A correct alignment could minimize stress concentration that result in loosening.

2.1.2.2 Knee Stability

The stability of knee joint depends on the special geometry of the bony structure, the constraint and balance of cruciate ligaments and the strength of extensor apparatus, quadriceps and hamstring. Most of the designs of knee implant rely on the stability of anatomical structure, especially the medial and lateral collateral ligaments.

2.1.2.3 Patello-femoral Joint

Patella is an important component of extensor apparatus in increasing the moment arm of quadriceps. Though irregular, patella has numerous quantifiable geometrical features, including size, thickness, articular surface geometry and location. The Chinese anthropometry of these patella features is different from that of westerners. These features would affect the patella implant design, both in terms of geometry and alignment.

In fact, the force vector of quadriceps and tibial axis form a varus angle, Q-angle (**Fig. II-7**), thus, patella tends to dislocate laterally. In OA patient also with degenerative patella, the lateral ligament is often stressed and the patella tends to be subluxed laterally. An implant design in consideration with degenerative patella

and ligament release protocol is important to reduce the risk of patella dislocation in these patients.

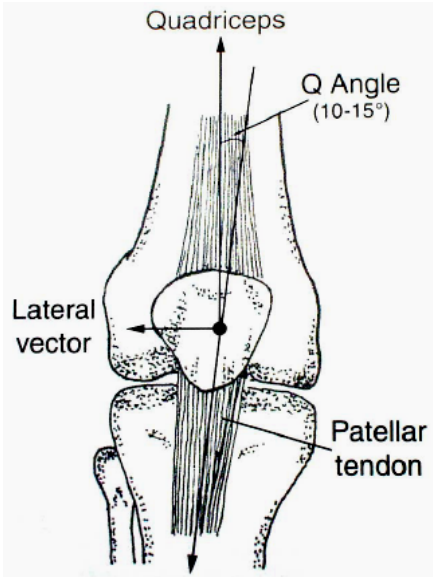

Fig. II-7 Q-Angle and the lateral force vector showing tendency of patella dislocate Laterally (Wu & Wu, 2005)

2.2 Knee Joint Biomechanics

2.2.1 Knee Joint Loading

Knee joint sustains large loading in daily activities. The magnitude of loading depends on the type of activities (level walking, running, stair-climbing), or deformity (valgus/varus, tibial bowing), and personal characteristics (walking habit, pace, body weight).

Knee joint loading changes with gait and posture. In balanced standing, knee joint loading is about 0.43 time of body weight and increase to 3.22 times of body weight upon walking. Stair-climbing could reach to 4.25 times of body weight. In walking, the instance after initial contact has a large knee loading and reaches to a peak at loading response. At terminal stance, the knee sustains large shear and torque.

The hypo-elastic properties of meniscus and cartilage could maximize the contact area between the femur and tibia, and thus lower the contact pressure. In single limb support, the center of mass of body run medial to the knee and requiring the tensor fascia latae and gluteus maximus to maintain balance. This causes an uneven load distribution on the tibial plateau, leading to knee varus and valgus.

2.2.2 Knee Kinematics

The normal range of motion of knee is about 145° flexion, with a maximum voluntary flexion of about 135° and maximum passive flexion of about 160°.

The knee flexion and extension is based on instaneous centre of rotation and also a combination of gliding and rolling. The motion is bought by the geometry of the femoral condyles and the effect of cruciate ligaments.

In the initial knee flexion at 0° to 25°, primary rolling of femoral condyles on tibial plateau occurs. As flexion continues after 25°, the displacement of the condyles tightens the cruciate ligament and creates an anterior translational force on the femoral condyles. The gliding action is further facilitated by the uphill geometry of the meniscus. The femur condyles simultaneously roll and glide on the plateau to keep from running out posteriorly. Extension of the knee from flexion is essentially a reversal of these actions.

The medial and lateral rotation of knee joint is preceded by a medial pivot at the medial condyle with a greater arc motion at the lateral condyle. The medial tibial condyle shifts slightly anterior, while the lateral tibial condyle shifts posteriorly at larger distance upon tibial lateral rotation. Tibial medial rotation is the reversal of the action. The maximum rotation angle is available at 90° knee flexion, with approximated 0-20° lateral rotation and 0-15° medial rotation. A slight abduction and adduction is also available at knee joint. The maximum abduction angle of 13° appears at 20° of knee flexion and there exists 8° abduction ranges at full extension. Tibio-femoral motions indeed are not pure motion and occur as a coupled of motions due to the oblique axis with respect to the tibial plateau level. Flexion is considered as a combination with varus motion, while extension is coupled with valgus motion.

2.2.3 Kinematic Stability

The stability of knee joint is attributed from: geometry of meniscus and the articular surface; soft tissue around the knee joint; ligaments and synovial cavity. In terms of dynamic stability, muscles provide knee movement, sustain external force and stabilize the knee joint. To balance the valgus/varus loading, MCL sustains 57.4% load. Upon extension, cruciate ligaments sustain 22.2% load at 5° of flexion.

2.2.4 Locking Mechanism of Knee

There is an involuntary terminal rotation at the final stage of knee extension to provide extra stability upon standing. The action originates from shorter lateral tibial plateau. During the last 30% of knee extension, the lateral condyle terminates the roll-glide action before the medial condyle. The medial condyle continues to roll and results in lateral rotation of tibial to femur. The motion results in tension of ligaments and lodging of tibial tubercles in the intercondylar notch and configured into a close-packed or locked position. The unlocking mechanism is produced by lateral rotation of femur to tibial before flexion.

2.2.5 Kinematics Features of Knee Implants

Although implant designers tries to mimic the geometry of knee and aims at reproducing physiological kinematics, the knee after TKA is very different from that of normal knee. First of all, knee requiring a surgery is not a normal knee, and may undergo pathological deformity. Secondly, the geometry of knee implant system is different, primarily aiming at pain-relieving and constructing simple mechanical axis for motion.

Tibial rotation is an important issue in TKA kinematics. Previous simple implant designs were symmetrical and restraining tibial rotation. The torque of restrain would result in mechanical loosening, while the pressure of medial and lateral side could not be evenly distributed due to the constraint. The load would shift from time to time leading to material fatigue.

Implant stability relies on the anatomical stability of knee structure, thus, surgeons often face the decision of ligament sacrificing. After TKR surgery, the anatomical stability from the geometry fitting of menisci-condyle complex is destructed. If the cruciate ligament is sacrificed, the dynamic stability, as well as proprioception is also lost. Together with the wounded muscles and soft tissue due to surgery, the anatomical stability is lost and the stability from implant design would be demanding. However, increasing internal stability of implant would transmit larger load to the bone and implant interface, leading to mechanical loosening. Compromising anatomical and implant stability could achieve a better surgical outcome and preserving as much anatomical features viable could provide a better knee joint stability.

2.3 Review of Implant Designs

2.3.1 Existing Knee Design Features

There are various designs of total knee joints available in the market. However, those designs are mostly various combinations of different design features. They can be classified in terms of fixation method: cement or cementless, and PCL retaining or substituting.

The use of cement and cementless fixation is controversy. PMMA cement was reported to be a good anchoring substance for knee implants (John, 2001). The operation of cementing is easy and it could repair minor irregularities between the implant and bone interface. However, some studies showed that the drawbacks of cementing outweighed cementless fixation. Besides poor transmission on mechanical stress (John, 2001), physiological problems, such as impairment of chemotaxis and phagocytosis, existed (Jones et al., 1987). Researchers strike for uncemented TKA and Scott et al. (1997) reported 95% component survivorship at 212 knees after 7-11 years using cementless fixation. With the advance of material technology, appropriate bone-implant contact could replace the function of cement. Cementless porous coating can provide confirming surfaces with no reported incidence of osteolysis (Whiteside, 1995).

PCL retaining and substituting design of knee implants were both showing excellent performance. Both designs had literatures proven to be better in stability, survivorship and kinematics than their counterparts (Sandeep & Kenneth, 2001; Steven & Khalin, 2001). While the selection on PCL retaining or substituting is controversial, PCL retaining designs were reported to have improved proprioception (DelValle et al., 1998) and PCL substituting designs can facilitate easier surgical exposure (Steven & Khalin, 2001). PCL substituting designs could be a better indication for major deformity, subluxed knee and residual translation stability (Sandeep & Kenneth, 2001).

Nowadays, some design approaches involve customization of patients' knee to produce the geometry of the implant. However, practicability and functionality may not be compromised. The methodology of customization is based on some of the reversed engineering techniques detailed in section 3.1. In fact, total knee arthroplasty has been developed for a hundred year. Extensive research has been done to examine different designs and geometry to produce the best implants in terms of their contact, kinematics and thus longevity. Researchers strive to enhance the fitness and geometry of the implant in view of reducing complications

due to mismatch. Another research area is to enhance the quality of the material and finishing aim at improving implant longevity.

2.3.2 Development and History of Knee Implants

The surgical resection by Fergusson in 1861 provided new treatment option to OA patients. In 1863, Verneuil inserted an artificial sac, using pig bladder, to avoid knee joint fusion. In 1940, Smith-Peterson made use of metal insert to replace animal tissue sac. However, pain-relieving effect was not satisfactory.

Hinge design knee implant was developed by Waldius and Shiers in 1950s with short-term success. Hinge design with single axis could allow flexion and extension of the knee joint, which improved the functional limitations of a joint sac. However, Metal-to-metal interface resulted in high wear rate. The over constraint on tibial rotation, abduction-adduction also resulted in loosening.

The second generation of implant was improved by Gunston in 1971 with better kinematics. The concept of rollback was imposed and could facilitate instantaneous centre of rotation and sliding. The design came to failure due to poor fixation. In 1973, Mayo clinic invented the Geomedic knee implant (**Fig. II-8**A). The Geomedic knee was designed with geometrically accurate femur shapes which increased stability of the knee joint. However, joint motion was not natural unless sacrificing the PCL.

In 1973, the total condylar knee (**Fig. II-8**B) developed by Insall proposed a new kinematics principle. They believed that producing natural joint movement was more important than geometrically accurate implant. The resurfacing of contact surface increased stability by ensuring congruity. The reduced posterior radius could also facilitate deep flexion. The principle of Insall imposed high impact to the current implant design.

In 1976, Goodfelow and O'Conner developed the Oxford knee implant. The implant consisted of a plastic insert on to a metal backing. The design incorporated better mobility and reduced tibial component wearing. Beuchel optimized Oxford knee and developed the LCS knee (**Fig. II-8**C). LCS controlled AP shifting of the insert and allowed axial rotation on the metal bearing. The LCS had the advantages of low contact stress, wear, increase in range of motion, and produced natural joint motion of which becomes the base of design nowadays.

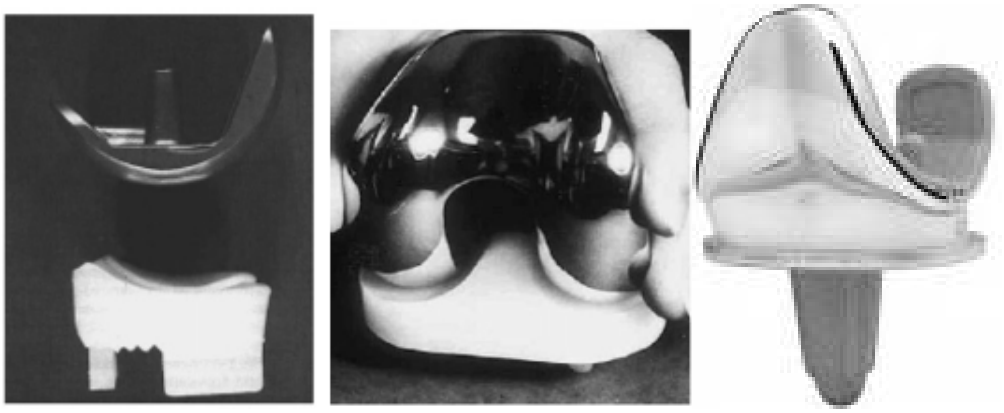

A) The Geomedic Knee B) The Total Condylar Knee C) The LCS knee

Fig. II-8 Some of the original knee implants models (Carr & Goswami, 2009)

Liow and Murray underwent a review and reflected TKA available in the United Kingdom by 1996. The below data (**Table II-1**) was extracted from primary and total knee while that of Liow and Murray included revision and uni-compartmental prostheses. Based on this review, there were 5 implants newly introduced before 1980, 12 introduced between 1980 and 20 since 1990.

The author discovered that 20% of TKR underwent major design changes, while other only taken minor modifications. The author doubted about the performance of “improved” design. Clinical evaluation was difficult and required long-term trials, whereas frequent modifications made assessment infeasible. It was also shown that 54% of TKR has not undergone strict testing. The author doubted the safety and quality of the implant and foreseen upcoming CE standard in Europe.

The testing of implant becomes more important as the use of multiple modular designs and frequent modifications made analysis more difficult. At this stage, manufacturers apply similar implant material, while some advance to use porous material. Design often focuses on improving the articulation between the femoral and tibial components for better wear reduction. Asymmetrical femoral components show the focus of designers on the natural geometry of femur. Functional-based and anatomical-based were still both the two major design principles.

Table II-1 Extracted data of TKR on the UK market in 1996 (Liow & Murray, 1997)

Manufacturer	Implant	Implant Type	Special Design Features
3M	Condylar Knee, 1993	Cemented	Asymmetrical Femoral Component Low Congruence
	Hybrid Condylar Knee, 1996	Cemented Tibial, Uncemented Femoral	Asymmetrical Femoral Component with Ultrapore ™ surface
Asculap	Blauth, 1985-1991	Hinged, Stemmed Cemented	Fully Constrained Fully Congruent
Biomet	AGC, 1983-1986	Modular or Monobloc Cemented or Cementless	Symmetrical and Asymmetrical Femoral Component
	Dual Articular, 1990	Cemented	Modular for Complex Primaries or Revision Semi-constrained Rotating Tibial Plateau Asymmetrical Femoral Component
Conrin	Minns, 1984	Cemented or Cementless	HAP or Porous-coated Cementless Asymmetrical Femoral Component Highly Congruent
	Rotaglide, 1986	Cemented or Cementless	HAP or Porous-coated Cementless Asymmetrical Femoral Component Rotating and Gliding Meniscal Component Highly Congruent
	Nuffield, 1988	Cemented or Cementless	HAP or Porous-coated Cementless Asymmetrical Femoral Components Highly Congruent Bone-preserving Intra- or Extramedullary Instrumentation
Depuy	LCS, 1985	Cemented or Cementless	Meniscal and Rotating Bearing Platform Options Congruent Rotating Patella
	AMK, 1987-1990	Cemented or Cementless	Matched Semi-congruent Femoral and Tibial Articulating Surface Unique Instrumentation Proportionally sized asymmetrical Femoral Component for

			Patellofemoral Function
Fry	Insall Burstein II, 1988	Modular Cemented Posterior Stabilized	Interchangeable Tibial Inserts, Wedges and Stems High Congruence
	Scan Knee, 1988-1996	Modular Cemented	Non-anatomical
Howmedica	Total Condylar, 1974	Cemented	Symmetrical Femoral Component
	Kinemax, 1988	Modular Cemented or Cementless	Symmetrical Femoral Component Offset Dome Patella
	Duracon, 1990	Cemented or Cementless	Asymmetrical Femoral Component Asymmetrical Patella Intra- and Extra-medullary Alignment
Johnson & Johnson	P.F.C. Knee, 1984-1989	Modular Cemented or Cementless	Four Levels of Congruence With Stems, Wedges & Augmentation Components
	Insall Burstein Posterior (IB I), 1978-1980	Cemented, Posterior Stabilized	Symmetrical Femoral Component Low Congruence
JRI	Furlong, 1994	Modular, Cement or Cementless	J-shaped Femoral Component Anatomical Kinematics
New Splint (Waldamar Link)	Endo-Model Total Rotational Knee, 1983	Cemented or Cementless	Modular with Stemmed Components Semi-constrained Rotating Hinge Congruent Surfaces Asymmetrical Femoral Component
	TACK, 1988	Cemented or Cementless	Bicondylar Asymmetrical Femoral Replacement Rotating Tibial Platform Congruent in Extension
Smith Nephrew Orthopaedics	Tricon, 1984-1987	Non-modular Cemented or Cementless	Asymmetrical Femoral and Tibial Components Domed Patella Congruent Articulation
	Genesis, 1988-1990	Modular Cemented or Cementless	Asymmetrical Femoral Component Biconvex Patella
	Profix, 1994-1996	Modular System	Asymmetrical Femoral and Tibial Components

		Cemented or Cementless	External Rotation Built into Articular Insert Biconvex Patella
Stratec	Freeman-Samuelson Modular Knee, 1990	Modular Cemented	Asymmetrical Femoral Component High Congruence Intra- or Extramedullary Alignment
	Freeman-Samuelson Integral Knee, 1995	Monobloc Cemented	Asymmetrical Femoral Component High Congruence Intra – or Extra-medullary alignment
	Wallaby, 1994-1995	Modular Cemented or Cementless	Asymmetrical Femoral Component Load Distribution Principle High Patellar Congruency Extra- or Intramedullary Alignment
Zimmer	Insall Burstein II, 1987	Modular Cemented Posterior Stabilized	High Congruence
	Miller Galantie II, 1990	Modular Cemented or Cementless	Anatomically Shaped Multi-radius PMMA Precoat or Porous
	NexGen, 1996	Modular Cemented	Posterior Stabilized or Constraint Options

From the summarized design data, most of the implants were using asymmetrical femoral component, aiming for better fit on distal femur. The designs of articular surface processed with high congruency for less stress concentration and better wear reduction. Manufacturers also developed system that was modular and interchangeable to cope with different patient requirements, such as cement and cementless, PCL retaining and scarf icing, patella geometry and alignment instrumentation.

Today, manufacturers previously had joint ventures or have been bough out by competitors. The table below (**Table II-2**) lists the common knee implants and their manufacturers. The data are extracted and arranged on September 2009 from manufacturers' websites. The summary includes primary total condylar knee and does not include revision and uni-compartmental prostheses. Nowadays, implant underwent strict standard and quality assurance. Most of them complied with ISO or ASTM standard, no matter on implant performance, sterilization and packaging. A lot of the designs provided material testing report, showing reduction in wear and material longevity. Some of them included experiment and finite element results to show their excellences on stress distribution and kinematics.

Implants were designed with modulation with different sizes and designs of different components to suit people with different knee sizes and demand. Some provide options on special features, such as porous coating and computer assisted surgery. In terms of design, both anatomical and functional, or a combination of both were the major design principles. Manufacturers focus on anthropometric designs to female, of which showing a greater demand, while still claiming compromise with male population. Deep flexion is another design trend, that more young adults with high demand of living could now gain benefit from the longevity of implants.

Table II-2 Extracted Data of TKR of common implant manufacturers in the market

Manufacturer	Implant	Special Design Features	Special Modular Feature
Aesculap Implant System Inc.	Columbus AS Knee System	Designed for Computer Navigation surgery Designed for Minimally Invasive Surgery	OrthoPilot Navigation (Computer Navigation Surgery)
Biomet	AGC Total Knee System	Improved Patella Alignment and Tracking	Regenerex Porous (Porous Coating)
	Ascent Primary Knee System	Improved Patella Alignment and Tracking Deep Flexion	Regenerex Porous (Porous Coating)
	Maxim Primary Knee System	Special Design Tibial Component Reduce Micro-motion	Regenerex Porous (Porous Coating)
	Vanguard Complete Knee System	With Numerous Modular Combinations	Regenerex Porous (Porous Coating) Signature Personalized Patient Care (Surgical Planning, Registration with MRI)
Johnsons & Johnsons Depuy Orthopaedics	LCS Complete Knee System	Deep Flexion	
	Sigma Knee System - CR - PS - High-Flex - RP	Deep Flexion Strong Bond and Fit Decrease Micro-motion Rotational Freedom Shear-decoupling Self-aligning Platform for High Activity Demand	Porocoat® (Porous Coating) Rotating Platform
Smith & Nephrew Inc.	Journey Bi-cruciate Stabilized Knee Systems	Normal Shape-Position-Motion For High Level Activities	Visionaire (MRI/X-Ray Alignment) Achieve CAS (Computer Assisted Surgery)
	Profix Knee System	Design for Instrumentation Simpler Surgical Technique Improve Surgical Accuracy	Visionaire (MRI/X-Ray Alignment) Achieve CAS (Computer Assisted Surgery) OXINIUM (Oxidized Zirconium Coating)
	Genesis II Total Knee System	Improved Patella Tracking Anatomical Design	Visionaire (MRI/X-Ray Alignment) Achieve CAS (Computer Assisted Surgery) OXINIUM (Oxidized Zirconium Coating)

Stryker Orthopaedics	Triathlon Total Knee System	Anatomical Design Deep Flexion Anterior Flange Reduce Notching	X3 Advanced Bearing Technology (Strength, Wear and Resistance)
	Scorpio NRG	High Rotational Allowance Reduced Bone Resection	X3 Advanced Bearing Technology (Strength, Wear and Resistance)
	Scorpio Single Axis	Increase Quadriceps Efficiency Reduce Anterior Pain Maintain Uniform Ligament Tension	X3 Advanced Bearing Technology (Strength, Wear and Resistance)
Wright Medical Technology Inc.	Advance - Stature Knee - Double High - Medial Pivot	Anatomical Design Deep Flexion Normal Kinematics Maintain Ligament Tension	Prophecy Pre-Operative Navigation
Zimmer Orthopaedics	NexGen - NR - PS - Flex-Fixed	Anatomical Design Deep Flexion	

Due to the biomaterial technology breakthrough, much of the implant manufacturers designed porous coating for implant to enhance bone ingrowths that reduce loosening. On the other hand, surgical deviation is another major cause of implant failure, thus computer assisted navigator using customization data on surgery simulation, alignment and implant selection is another trend of implant development. On the long run, this customization could also assist in optimizing implant shape and design for better fit and performance.

2.3.3 Asians and Westerners Parametric Difference

Different implant manufacturers have been modifying their products' geometry in view of demonstrating best fit to patients. They researched on the anthropometric differences of gender and produced a gender-specific solution, while overlook the effect of ethnicity.

Ho et al. (2006) underwent research to evaluate five prosthetic systems: Duracon and Scorpio (Stryker Howmedica Osteonics), NexGen (Zimmer, Warsaw, Indiana), PFC Sigma (Depuy-Johnson and Johnson, Warsaw, Indiana) and UKnee (United Ortho Co., Taiwan). With the given main parameters AP dimension, the NexGen, Duracon and UKnee systems tended to overhang the ML condyles. The authors demonstrated that many of the systems that suitable for use in Caucasian patients may not be suitable for Chinese patients.

In fact, investigations were carried out to prove that Chinese knees were different from that of westerners. Sun et al. (2002) showed that the parameters of Chinese knees are similar to that of Indians and Japanese, which fell into the size "SMALL" and "VERY SMALL" category in selecting knee systems (Khoo et al., 1993). Nagamine (2000) made a detailed comparison on the anatomical parameters, showing that OA Japanese had a larger tibial angle and a larger angle between mechanical and anatomical axis (**Table II-3**).

Table II-3 Comparison of anatomic configurations with OA and normal knees (Nagamine, 2000)

	Japan (OA) *Nagamine, 2000*		Japan (Normal) *Kurosaka, 1994*		USA (Normal) *Moreland, 1987*		France (Normal) *Kapandji, 1986*
Parameter (degree)	Mean	SD	Mean	SD	Mean	SD	Mean
TA	97.2	3.8	95	2	93	1.6	93
Angle M-A	7.7	1.9	NM	NM	5.8	0.7	6
FA	81.9	2	80.2	2.2	81.2	NM	81

TA, tibial angle; Angle M-A, angle between mechanical axis and anatomic axis of the femur, FA, femoral angles; NM, Not Measured

In terms of alignment, Nagamine (2000) also showed that Japanese patients had much bowing of the femoral shaft and proximal tibial vara, with the offset of the tibial shaft with respect to the center of the tibial plateau. The mean anatomical knee axis was reported to be 5 degrees rather than that of 3 degrees in westerners (Wu & Wu, 2005). Furthermore, the posterior slope of tibial plateau in Chinese was 11.5 degrees rather than 5-10 degrees of western literature (Chiu et al., 2000).

2.4 Review of Existing Finite Element Analyses of Implants

2.4.1 Introduction to Finite Element Analysis

Finite element analysis (FEA) is a numerical method in solving partial differential equations and integral equations. The technique based on standard numerical algorithms such as Euler and Runge-Kutta.

FEA was firstly used in solving structural problems in civil and aeronautical engineering. With the advance of computer technology, the method becomes feasible in simulating complex geometry, sophisticated material properties, and nonlinear behavior, of which very useful in biomechanical applications. FEA provides a mean in investigating the internal stress and deformation of anatomical structure whereas in vivo experiments are not viable. Researchers could study various responses with different parameters and conditions which aids in studying pathological etiology in terms of biomechanics and help in design and establishing treatment plans.

FEA consists of pre-processing, solution and post-processing stage. In the pre-processing stage, users are required to define the problem by providing geometrical structure of the model, material properties, loading and boundary condition of the scenario. The solution stage could be achieved by the computer via commercial package such as ABAQUS. Users required minimal participation unless solution could not be yielded by default parameters. Finally, the results could be studied on the post-processing stage, where different physical variables such as stress and strain would be displayed and interpreted.

The principle of iteration scheme and solution control in the solution stage is described in ABAQUS manual. Considering the external forces **P** with internal forces **I** acting on a body (**Fig. II-9**), the net force must be zero to achieve equilibrium condition (**P – I = 0**).

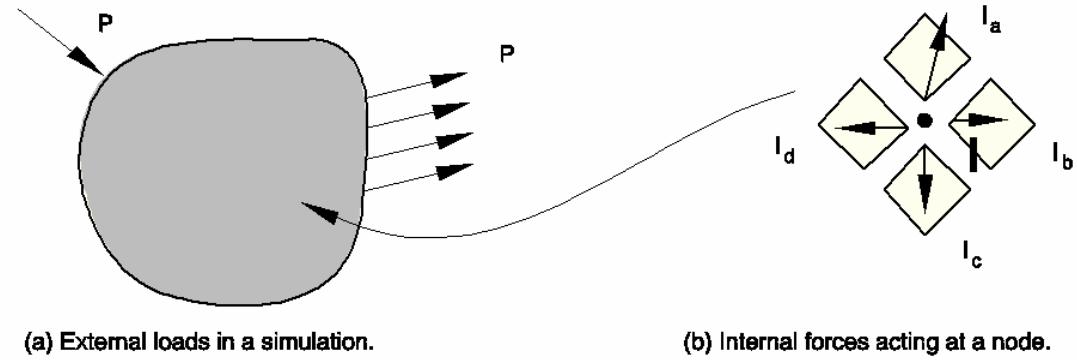

Fig. II-9 External and Internal Loads on a body (ABAQUS, 2004)

A small load increment **ΔP** by nonlinear response of the structure would result in displacement and change internal forces (**Fig. II-10**). The difference by the applied load is now updated to $\mathbf{R_a = P - I_a}$ where $\mathbf{R_a}$ is the force residual for the iteration. When the structure is at equilibrium, $\mathbf{R_a}$ is zero at every degree of freedom in the model. However, it would never be exactly zero in a nonlinear problem. ABAQUS accepts the solution as being equilibrium when $\mathbf{R_a}$ is less than a tolerance value. Another convergence criterion is checked with $\mathbf{c_a}$ greater than a fraction of $\Delta\mathbf{u_a}$.

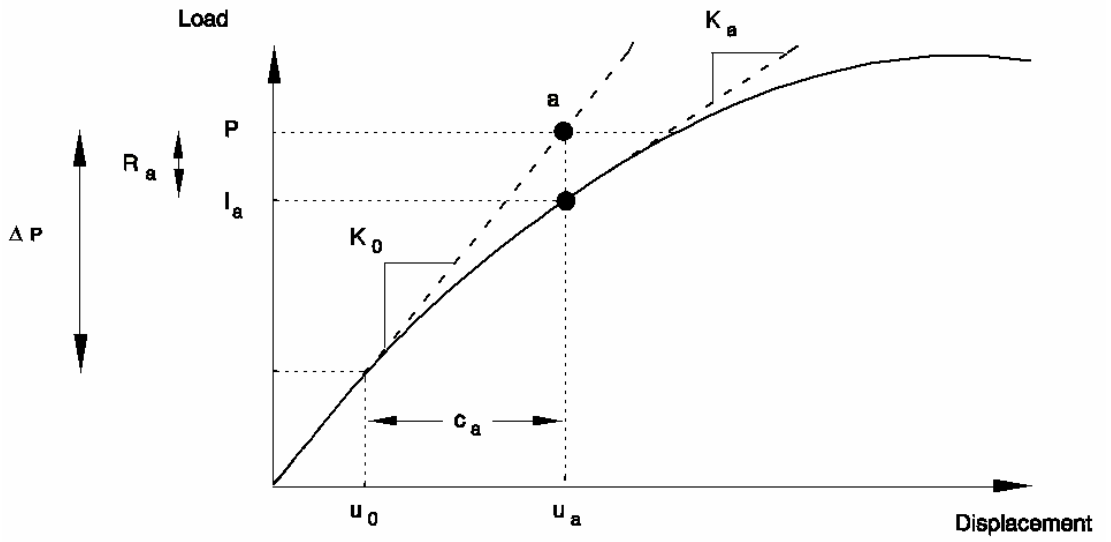

Fig. II-10 Iteration scheme in an increment (ABAQUS, 2004).

If the solution does not converge, iteration would be performed with smaller increment and try to bring the internal and external force into balance within tolerance. The increment size may need to be reduced and the calculation may need to be reiterated by highly nonlinear problems.

2.4.2 Review on Existing Finite Element Models

2D models were reported developed by Chu (1999) to monitor the performance of knee implant at single plane perspective. 3D simulations had also made with combinations of 1D, 2D and 3D structure to represent different structures for sake of reduced computational cost (Beillas et al., 2004). Researchers simplified their models by using simple beam element on ligaments to allow easier modeling and FEA processing (Penrose et al., 2002).

Some research focused on particular portion of the knee to precede a more specific analysis. In the study of Song and his colleagues (2004), their model assumed rigid behavior of bones, and put extensive effort on analyzing the ligaments by giving it more precise material properties. Ferandez and Hunter (2005) presented a setting with internal patella stress and quadriceps extensor forces to analyze the main features of patella biomechanics.

Geometrically accurate and detailed models were also considered. One of the examples was the model of Haut Don Chue et al. in 2002. The models included both trabecular and cortical bone of femur and tibial, ligaments and articular cartilage. Kim et al. (2008) and Completo et al. (2008) developed FE model with considerations of detailed geometry and material properties of bone to evaluate

design features of implants.

Most of the simulations underwent implicit solver in dealing with static and quasi-static scenarios, of which producing accurate results from non-linear input, such as material properties and surface interactions. In fact, Godest et al. (2002) carried out explicit FEA to simulate gait cycle and Halloran et al. (2003) modeled total knee biomechanics with explicit solver. Explicit FEA proceeds with small time step, in advantage of dealing with relative dynamic conditions, such as impulse simulations.

In terms of mesh type, tetrahedral and hexahedral elements were commonly used in 3D simulations. In fact, combinations of these two kinds of elements were also demonstrated. Tetrahedral element could model more sophisticated geometry with higher conformity whereas hexahedral components are more computationally feasible and produce better results in calculating load transfer in surface interaction conditions. Thus, hexahedral elements were often used on the tibial insert components. Spring elements were used to act as constraining structure, such as ligaments in the model. Besides, Liau et al. (2002) modeled Fuji film with plane strain elements to assess the actual contact characteristics of experiment with the film.

Upon material properties used in models, existing literatures showed much diversity. Relative simple analysis regarded metallic component as rigid due to its higher elastic moduli, compared with that of polyethylene and bones. Most of the implant femoral components were made of titanium or cobalt alloy with elastic moduli ranged from 110 to 200 GPa and Poisson's ratio from 0.3 to 0.34. UHMWPE generally had a lower elastic moduli compared with that of bone, ranged from 0.5 to 8.1 GPa. Some complicated material models were also reported. Godest et al. (2002) and Halloran et al. (2005) both applied a true stress-strain relationship on the tibial components. Moreover, Villa et al. (2004) made used fourth-order constitutive material characteristics on the tibial components.

Due to the limitations of computer technology, previous FEA often focused on analyzing implant and omitted bone and other anatomical structures. Recent research included bone structures, with both trabecular and cortical division to study the interactions between bone and implant (Beillastic et al., 2004; Miyoshi et al., 2000) the elastic moduli of cortical bone ranged from 8 to 17.5 GPa, whereas

that of trabecular bone ranged from 0.45 to 1.5 GPa, with Poisson's ratio 0.3 and 0.2 respectively. With advance of medical imaging, the material properties of bone are now detected by apparent density of bone images. Kim et al. (2008) and Travis et al. (2009) made used of this methodology to evaluate implant design parameters on bone stress.

Most of the FEA fixed one base of the models and applied load at the other end, while some allow limited femoral and tibial motion. Bone ingrowth and cementation surface interaction were applied in Miyoshi et al. (2002) and Villa et al. (2004) research model respectively. About 2000N load was applied in most of the studies, at an assumption of two to three times bodyweight of an 80kg person, simulating largest load upon walking. Typical flexion angle: 30, 45 and 60 degrees were simulated to access stress distribution at various instances. In simulating gait cycle, Godest et al. (2002) and Halloran (2005) varied the load magnitude and location in explicit FEA. The condition applied was based on the mechanical environment of the Stanmore knee simulator. No human subject experiments were conducted to validate FE results, despite some in vitro experiments were demonstrated.

The geometry of implant and bone components were seldom reported. Most of the FEA reported the type and manufacturer of the knee implant. In fact, Kim et al. (2008) reported the size of the implant with details in dimension modifications, together with measurements of bones. Travis et al. (2008) also reported the size of implant as well as the ranking of bone density. **Table II-4** shows a summary on existing FEA.

Table II-4 Summary of FEA settings in literatures extracted from Carr & Goswami (2009)

Author/Year	Manufacturer/Type	FEA Type	Material Properties			Element Types	Boundary Conditions
			Component	E(GPa)	*v*		
Chu, 1999	NJLCS Knee, Depuy (Johnson and Johnson)	2D	Femoral UHMWPE	110 0.6	NR NR	Tetrahedral	2200N Uniformly Distributed Flexion Angle:0, 60, 90, 120 Varied in Gait Condition Bottom Surface Fixed
Miyoshi et al., 2002	Muller-Galantie II, Zimmer	3D	Tibial UHMWPE Cortical Cancellous	112 8.1 8.0 1.5	0.34 0.4 0.3 0.2	Hexahedral	2-1000N Concentrated Compressive Stance Phase Fixed on Bone Distally
Godest et al., 2002	PFC Signma Knee, Depuy (Johnson and Johnson)	Explicit 2D Femoral Component 3D Tibial Component	Femoral UHMWPE	Rigid True Stress-strain Curve	Rigid True Stress-strain Curve	4-node Shell Hexahedral	Varied in Gait Condition Max. Input Force: 2200N Torque: 7N (Internal) Translation: 200N (Posterior)
Halloran et al., 2005	NR	Explicit 2D Femoral Component 3D Tibial and Patella Component	Femoral UHMWPE	Rigid True Stress-strain Curve	Rigid True Stress-strain Curve	Triangular Hexahedral	Varied in Gait Condition Max. Input Force: 2300N Torque: 7.5N (Internal) Translation: 50N (Posterior)
Liau et al., 2001	U-Knee, United Orthopaedics	2D and 3D	Femoral UHMWPE Fuji Film	Rigid 0.50-0.91 0.10-0.15	Rigid 0.46 0.45	Rigid Element 8-node Brick 4-node Shell	900-3000N Indentation Allow Tibial Component Translation and Tilting
Liau et al., 2002	U-Knee, United Orthopaedics	3D	Femoral UHMWPE	Rigid 1.016	Rigid 0.46	Rigid Element 8-node Brick	3000N Fixed Tibial Component Base
Liau et al.,	U-Knee,	2D	Femoral	Rigid	Rigid	Plane Strain	300-3000N Indentation

2002	United Orthopaedics		UHMWPE Fuji Film	0.910,1.016,1.200 0.100	0.46 0.40		Fixed Femoral Component and Fuji Film Horizontally
Villa et al., 2004	Prototype	3D	Femoral Tray UHMWPE	200 200 Fourth-order Constitutive Relationship	0.3 0.3 0.45	Tetrahedral Tetrahedral Modified tetrahedral	Fixed Tibial Tray 2200N@15 Degree 3200N@45 Degree 2800N@60 Degree Fatigue Test:500,2000,4000N
Bartel et al., 1986	Insall-Burstein Knee	3D	Femoral UHMWPE	Rigid 0.514,Post-yield at 0.214	Rigid	NR	1500N, 3000N
Kim et al., 2008	Advance Revision, Wright Medical Technology	3D	Tray Cortical Cancellous	110 17 0.3	0.34 0.36 0.2	Tetrahedral	Fixed Bone Distally 2000N
Travis et al., 2009	NexGen, Zimmer	3D	Femoral Coating Load Yoke Bone	210 6.9 200 Based on Apparent Density	0.3 0.3 0.3 0.3	Tetrahedral	890N with Yoke to Interior Anterior of Femoral Component

Carr et al. (2009) commented that previous models often regarded femoral component as rigid and estimate constant Young's modulus and Poisson's ratio. Most of the studies only evaluated the response of tibial component, due to the common failure of wear. Despite these similarities, reported literatures could not be compared. This is due to the difference of specific model geometry, material properties and boundary conditions. However, the summary of these results could provide general trend and references to knee implant behavior.

Table II-5 FEA results summary extracted from Carr & Goswami (2009)

Author/Year	**Research Focus**	**FEA response Max Compressive stress**	**Max. Displacement / Rotation**
Chu, 1999	Contact Stress on Tibial Component	17.2MPa	NA
Miyoshi et al., 2002	Stress and Displacement of Tibial Component upon Different Component Shape	23.3MPa (von Mises)	NA
Godest et al., 2002	Contact Stress and Translation upon Different Mesh Density, Time Step and Friction	23.9MPa	4.3mm Posterior 6.1 degree Internal Rotation
Halloran et al., 2005	Contact Stress and Implant Kinematics	~20MPa	5.6mm Posterior 6.1 degree Internal Rotation
Liau et al., 2001	Contact Stress with Influence of Fuji Film	~32MPa (with film)	NA
Liau et al., 2002	Contact Stress upon Malalignment	Malalignment 80.2 (contact) 39.5 (von Mises)	NA
Liau et al., 2002	Contact Stress with Influence of Fuji Film	NA	NA
Villa et al., 2004	Contact Area and Stress Fatigue, Compared with Experiment	27.7MPa	NA
Bartel et al., 1986	Contact Stress of Tibial Component upon Component Conformity, Thickness and Material	~40MPa	NA
Kim et al., 2008	Contact Pressure and von Mises with Different Stem-end Designs	43.06MPa (stem-end)	NA
Travis et al., 2009	Contact Pressure and Principal Strain	16.5MPa	Largest Strain: -276με (Anterior Medial)

The maximum contact stress of the tibial component ranged from about 17 MPa to about 27 MPa. The maximum stress exceeded 10 MPa (Chu, 1999), the allowable stress, which defined as the suggested stress limit by manufacturers that incorporates a safety coefficient. It also marginally exceeded the yield strength of

UHMWPE, 27 MPa. This showed that the stress was marginally acceptable at a controlled environment. However, stress failure or fatigue may occur, especially in malalignment, of which about 80MPa (Liau et al., 2002) contact stress could be resulted.

2.4.3 Summary of Existing Finite Element Analyses

Because of computational advancement, 3D and detailed knee anatomical models could be reconstructed, with not only bones, but soft tissues. The FE models nowadays could simulate bone-implant complex environment to investigate the effects of bone on the factors concern. The material properties are not confined to single value. Some researches applied true stress-strain or constitutive relationship to model engineering materials. The material properties of bone can also be adopted by detecting the apparent density by clinical imaging.

Although bone-implant situation could be simulated, most of the studies still focused on the contact pressure of the tibial component, aiming at proving longevity of implant. In fact, much of the implant performance or failure could also be assessed at the bone-implant interface, such as loosening or stress shielding at the interface.

Explicit FEA was applied to simulate gait condition of knee implant. However, the result is sensitive to mesh density and time step, of which the accuracy would be in doubt. Implicit FEA in simulating gait condition could provide a more accurate solution especially involving multiple component interactions.

CHAPTER III METHODOLOGY

The design approach in general was to establish a platform from design to prototype manufacturing of knee implant (**Fig. III-1**). The process started with the reverse engineering of knee and implant model. The model was aligned together and simulated with surgical resection procedures in the model combination phrase. The research was then focused on FEA and the parametric study. The manufacturing process was collaboration with research partner and is not detailed in this thesis. This platform could aid in understanding clinical or design problems of implant, as well as discovering new features or clinical finding that could aid clinicians to optimize surgical decision.

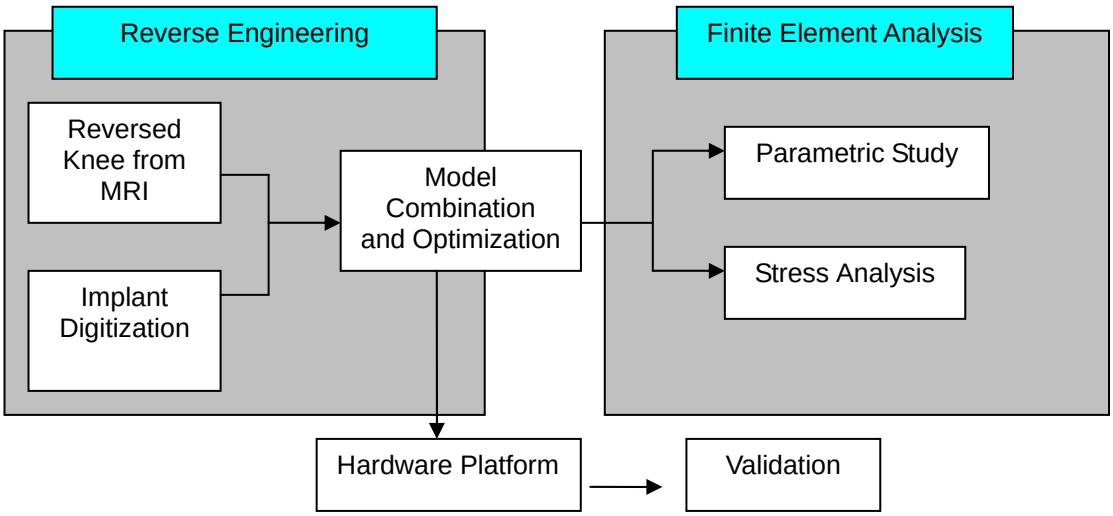

Fig. III-1 Workflow of the design platform

The upcoming paragraph would be divided into three sections. Firstly, the model reconstruction and optimization based on reverse engineering technique would be introduced. Secondly, the geometrical models would be combined and simulated with surgical alignment and resection. The models were then converted into FEA settings, by applying material properties, loading and boundary conditions, and mesh assignment. Finally, a parametric study by changing FEA input parameters would be discussed.

3.1 Geometry Reconstruction
3.1.1 Knee Model

Clinical images from MRI were used to acquire geometrical information of the knee joint. MR scan was done on a healthy female, aged 28, weighed 54kg, and of 165 cm tall, using a 3.0-T MR Scanner (Seimens, Germany) at 1-mm interval (**Fig. III-2**). The images taken were of right knee in neutral and non-weight-bearing condition. When taking the MR images, the subject had worn an ankle-foot-orthoses, so as to keep the foot at neutral position that in turn keeps the knee alignment. The subject had signed a consent form and well-introduced with the research purpose and procedures.

Fig. III-2 The MR images of the right knee were scanned with 1mm interval at transverse plane (Seimens, Germany)

The MR images were segmented using the software MIMICS (Materialise, Belgium). Trabecular, cortical bone and other soft tissue were identified to facilitate the setting of physical properties in different regions. The figure below (**Fig. III-3**) shows details of the bone model.

Femur Bone	
ML (dx)	71.9 mm
Medial AP (dy)	57.2 mm
Lateral AP (dy)	55.0 mm

Tibia Bone	
ML (dx)	66.9 mm
Medial AP (dy)	32.9 mm
Lateral AP (dy)	44.0 mm

Fig. III-3 Reconstruction of knee with measured AP and ML distance

3.1.2 Implant Model

Wright total knee system (ADVANCE® Primary) would be imported to establish and test the platform. Parametric study of FEA would be taken place based on this specific model. **Fig. III-4** and **Table III-1** show the location of implant component and its dimension.

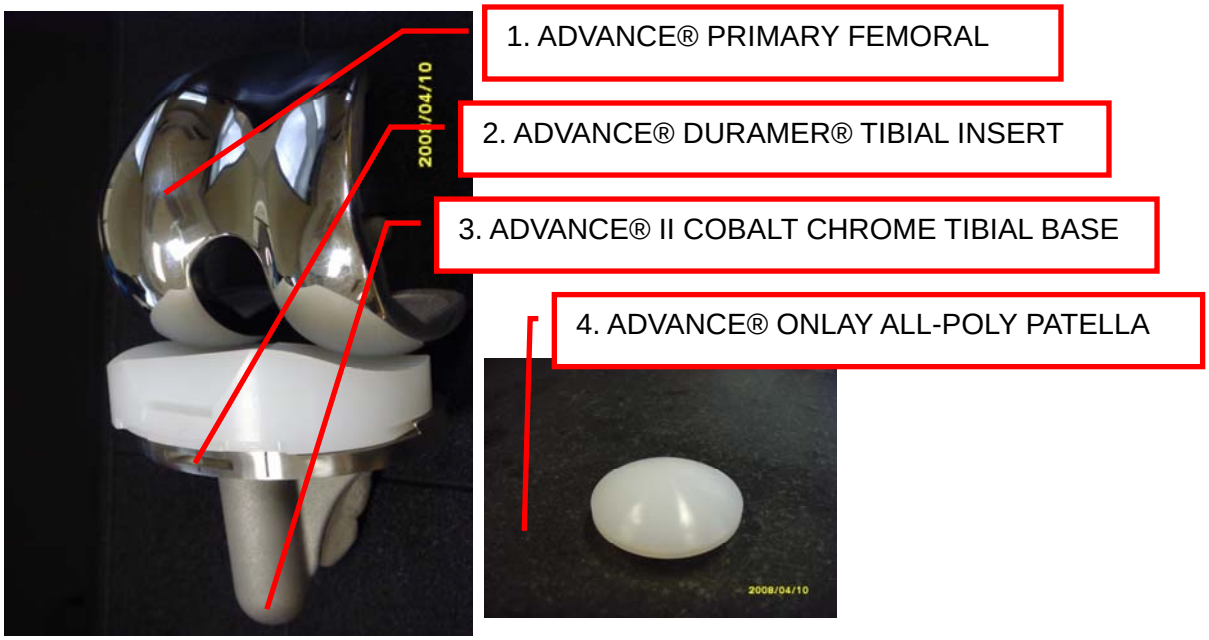

Fig. III-4 Location of different knee implant components

Table III-1 Dimension of femoral component and tibial insert

Femoral Component	Dimension
Medial - Lateral	64mm
Lateral AP	52mm
Medial AP	50mm
Base Max. Thickness	5mm
Stem	15mm Radius 3mm

Tibial Insert Component	Dimension
Medial – Lateral	66mm
Lateral AP	41mm
Medial AP	41mm
Condylar Thickness	12mm

A non-contact 3D scanner (**Fig. III-5**), Scan 3D II Precision (Frontier Advanced Technology Ltd., Hong Kong, China) was imported to facilitate the digitization of implant. The 3D scanner would capture the amplitude of the scanned item in a plane. Afterwards, the scanned item would be turned and other side of the item would be scanned. The scanned data were conditioned in the software, Scan 3D Pro (Frontier Advanced Technology Ltd., Hong Kong, China). The data were exported

into point cloud format to the software Rapidform XOV (INUS Technology Inc., Seoul, Korea). Registration and other signal processing would be taken place. The images of different planes would be put together and formed a merged volume.

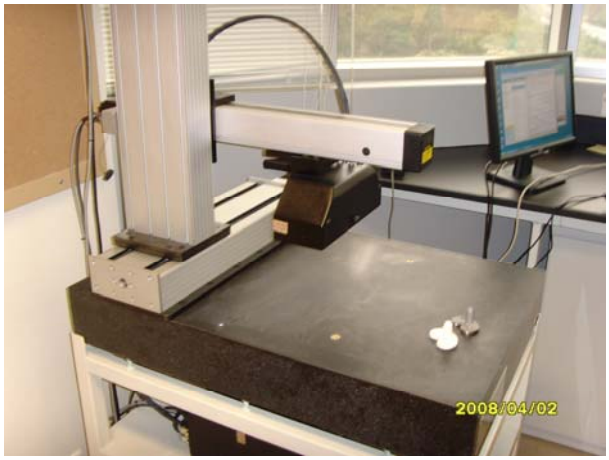

Model	Scan 3D II Precision
Scan Volume	380x300x320mm
Linear Accuracy	0.0125mm
Linear Repeatability	+/- 0.05mm
Optical Resolution	0.1mm(Z) 0.05mm(Y)
Laser Type	Class II laser, 670nm, visible red spectrum

Fig. III-5 Scan 3D II Precision with specifications

The merged volume data would then be exported into Rapidform XOR (INUS Technology Inc., Seoul, Korea). Primitives and control spines would be modeled based on the merged volume. Parametric model was formed to assist in the preceding parametric study.

3.1.3 Model Combination

After the geometrical reconstruction of the knee and implant model, the models were then imported to the software Rapidform XOR to simulate surgical alignment and resection. Some of the features of the implant, such as fillet and unnecessary boundaries, were simplified to facilitate better FE process. The model combination stage simulated the surgical resection procedure and aligned the implant with the bone. Since, this process depends on clinician's experience, the fixture of cutting device, as well as the knee alignment of the patients, universal alignment of the component is difficult to establish. The optimal position of the implant and knee in this research was established by the correlation operation of the software that gives a relative objective alignment process. By giving its reference orientation, the operation could match the two volumes, by calculating the best overlapping volume and exterior surface (**Fig. III-6**). The tibial component was titled afterwards to ensure the shaft of the tibial component aligned with the tibial shaft, making about 10° posterior slope of the platform, which described in the surgical guideline of the implant. The resection was done by the Boolean operation of the software. Afterwards, some cutting planes were formed by the internal surface of the implant. The bones were cut by these cutting planes to remove excessive bone that could not be removed by the Boolean operation. **Fig. III-7** shows the set of bone-implant complex after resection and alignment.

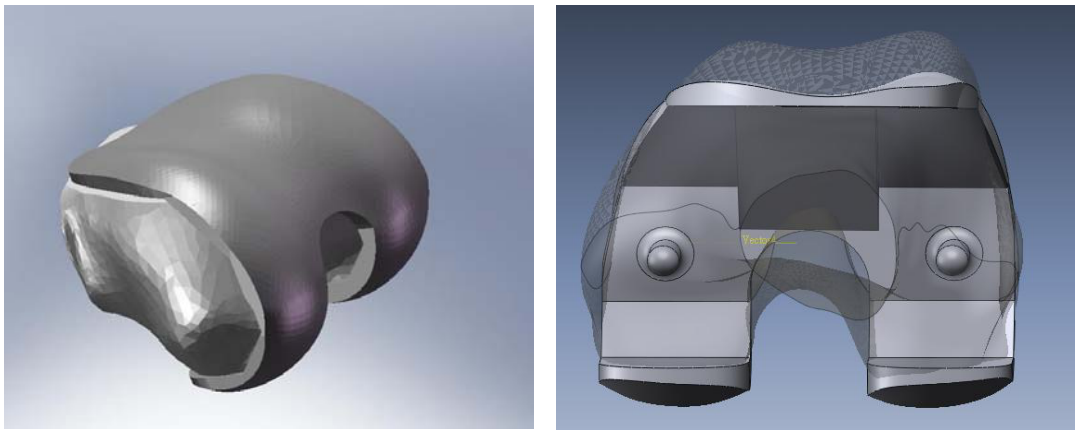

Fig. III-6 The bone was combined with the implant by the correlation function and resected by the Boolean operation and cutting planes, orientated view (left) and transparent view (right)

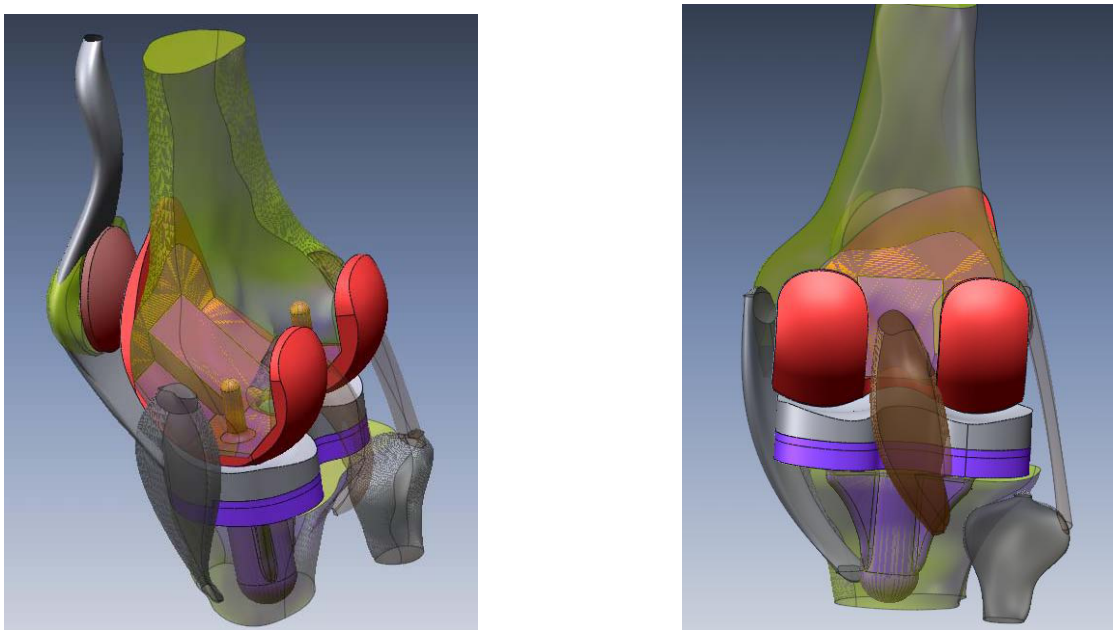

Fig. III-7 The bone-implant complex after the model combination, surgical alignment and resection, isometric view (left) and posterior view (right).

3.2 Development of the Finite Element Model

3.2.1 Material Properties

As shown in **Fig. III-8**, the implant consisted of the femoral component, tibial tray, and the tibial insert. The patella component would not be included in the simulation. The femoral component and tibial tray was made of titanium alloy, with elastic modulus and Poisson's ratio of 110 GPa and 0.34 respectively (Chu, 1999). The tibial insert was made of Ultra-high molecular weight polyethylene (UHMWPE), which had an elastic modulus and Poisson' ratio value of 8.1GPa and 0.46 (Miyoshi et al., 2002).

The material property of the cortical bone was assigned orthotropic (Ashman et al., 1984). Due to its relative rigidity to the trabecular bone, it was set consistent throughout the parametric study. The trabecular femur was assigned with a mean elastic modulus 389MPa (Rohlmann et al., 1980) and the trabecular tibia was assigned with 445MPa (Linde et al., 1989). Both of them were assigned with Poisson's ratio 0.2. The elastic modulus of the trabecular bone would be a variant throughout the parametric study. All components used 3D-tetrahedra as the element type. 3D-tetrahedra mesh is adaptive to complex and abrupt change of geometry. It is also a common and computationally cost effective mesh type in studying compression. Below shows a summary of the material properties of different components.

Table III-2 The material properties and element type of the FE model

Component	Element Type	Elastic Modulus	Poisson's Ratio	Number of Elements
Femoral Component (Titanium)	3D-Tetrahedral	110GPa	0.34	35452
Tibial Tray (Titanium)	3D-Tetrahedral	110GPa	0.34	25194
Tibial Insert (UHMWPE)	3D-Tetrahedral	8.1GPa	0.46	15966
Cortical Bone	3D-Tetrahedral	Orthotropic E_1, E_2, E_3, G_{12}, G_{13}, G_{23} 12,13.4,20, 4.5, 5.6, 6.2 (GPa)	v_{12},v_{13},v_{23} 0.38,0.22,0.24	18958 (femur) 8787(tibia)
Trabecular Bone – Femur	3D-Tetrahedral	389MPa	0.2	76589
Trabecular Bone - Tibia	3D-Tetrahedral	445MPa	0.2	54882

Subscript 1: radial direction relative to the long axis of the bone, 2: tangential direction, 3: longitudinal direction.
(Chu, 1999; Miyoshi et al., 2002; Ashman et al., 1984; Rohlmann et al., 1980; Linde et al., 1989)

3.2.2 Loading and Boundary Conditions

In this study, 2000N compressive force (Kim et al., 2008), which simulated 2.5 times body weight of 80kg adult, was applied on the bone and implant. This magnitude of compressive force could simulate the normal peak load required for activity and also commonly adopted in existing literatures. The compressive force would also be varied to test the sensitivity of load.

In the FE environment, two rigid ends were firstly defined at the proximal end of the distal femur and the distal end of the proximal tibial. This ensures better control for the force application and the degree of freedom, when preceded to more sophisticated conditions, such as gait. A static compression was achieved by restraining the rigid surface of distal femur and applying varying load in proximal femur. The load was 2000N as a starting standard in this study. (**Fig. III-8**). When studying the effect of flexion and gait, the restriction of distal femur was released, and the angular displacement of flexion angle was applied on the distal femur, while the angular displacement of the internal/external rotation angle was applied on the proximal tibial. Other degrees of freedom were released to allow the implant to move freely according to the contour between the femoral component and the tibial insert.

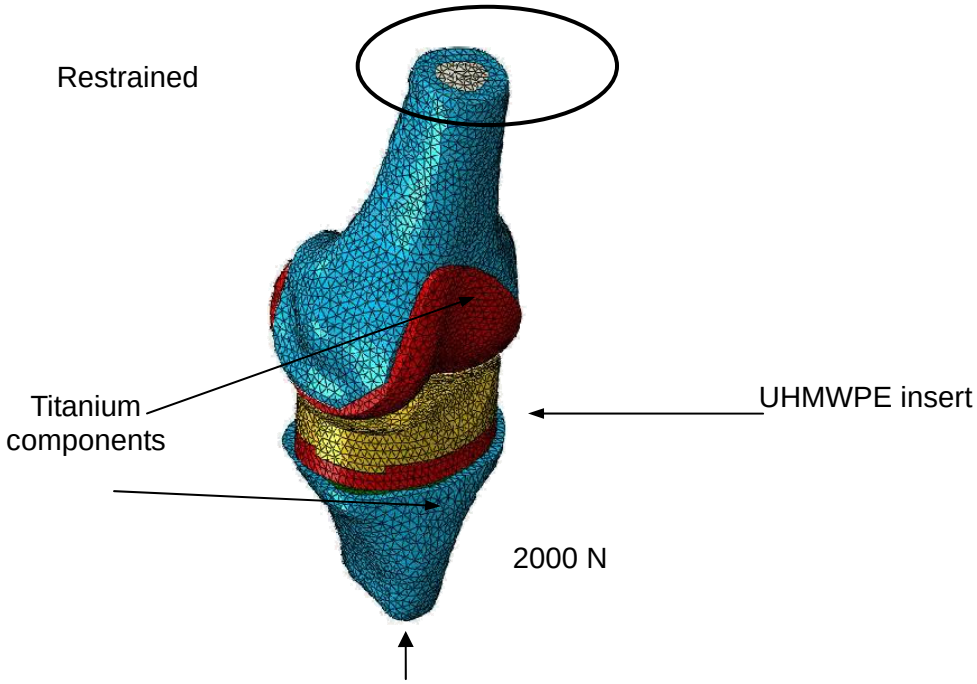

Fig. III-8 Load and boundary conditions for the FE model.

The trabecular and cortical core of the bone were modeled as one shell and there was no interface action between them. The bone and implant interface between the femoral component and resected femur, and between the tibial tray and resected tibial were tied. The coefficient of friction between the femoral component and the tibial insert was set to 0.07 (Godest et al., 2002).The tibial tray and tibial insert was tied together.

A gait simulation was also carried out using the FE implicit solver with quasi-static instance. The boundary condition of the gait was based on the International Standard Organization, ISO-14243-3, "*Implants for surgery – wear of total knee prostheses – Part 3: Loading and displacement parameters for wear-testing machines with displacement control and corresponding environment conditions for test*". The boundary conditions are as shown (**Fig. III-9**):

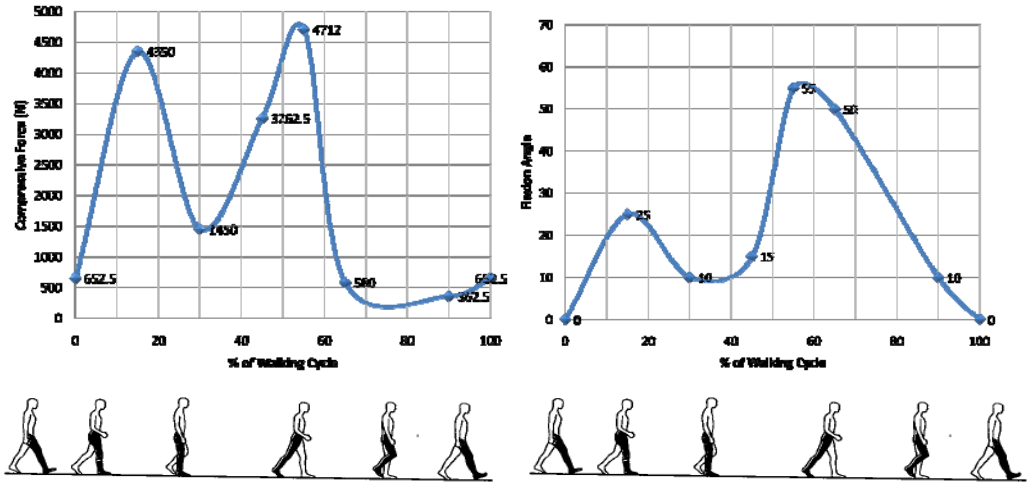

Fig. III-9 Compressive force and flexion angle in simulating gait condition (ISO)

Since the setting of FE was applying quasi-static, the steps of the simulations were set to assigned flexion angle and compressive force at discrete time instances in the input boundary conditions in order to monitor the changes at the least count of steps. Unlike the ISO standard, bones were also considered in the current simulation. As a result, the load was applied through the centre of the bone as an assumption, different from that of off-set applying to the implant. The steps were set as followed:

Table III-3. Step setting in FEA based on input boundary conditions of ISO-14243-3

Step	% Gait cycle	Flexion/extension Angle / Deg	Axial force/N	Tibial int. / ext. rotation / Deg
0	Alignment stage	NA	NA	NA
1	0	0	167.6	-1.57
2	3	1.53	1887.3	-1.7
3	7	7.16	1174.6	0.01
4	13	15.31	2600	1.09
5	16	15.96	2342	1.20
6	25	12.20	838.2	0.20
7	41	5.13	2281.2	-1.55
8	45	8.13	2433.5	-1.26
9	60	41.64	167.6	1.78
10	73	57.82	167.6	4.07
11	100	0	167.6	-1.57

3.2.3 Parametric Study of Knee Joint Setting

After the settings of FEA, parametric study was preceded to demonstrate the functions of the platform. The sensitivity of load was firstly taken place. The effect to varying load could allow basic assessment of the model, as well as verifying the results with existing literatures. 2000N, representing 2.5 times of 80kg adult was applied as a starting line. Analyses were made from 50% to 250% of starting load at 25% interval, of which the interval could reveal changes apparently.

The sensitivity of load study was crossed with different flexion angles to study the performance of knee implant at different common knee positions. Neutral position, 5-degree, 30-degree, 45-degree and 60-degree were set by applying angular displacement at the distal femur, together with compressive force at the proximal tibial.

The effect of varying bone stiffness was accessed to study the mechanism of periprosthetic fracture and stress shielding effect due to osteoporosis. The stiffness assigned in this study was converted to bone mineral apparent density (BMAD) for the sake of clinical interpretation of which BMAD is proportional to the bone yield stress (Travis et al., 2008). The yielding stress refers to the point of stress at which the material begins to deform plastically. While the exceeding the yielding stress, some fraction of deformation would be permanent and non-reversible.

Lastly, stress transfer parameter (STP) was established to evaluate the load transfer ability, as a method to access stress shielding. The effect of varying BMAD on STP would be studied to investigate the risk of loosening due to lacking of bone density.

3.3 Validation of Finite Element Model

Mesh convergence test was not carried out due to overwhelming factors, such as multiple interactions, relative large sliding, in the simulations, of which the convergence is not solely dependent on mesh density. In fact, the necessity of mesh convergence test is downfallen, due to the advancement of computer technology. The simulations nowadays precede mesh density sufficient for a converged result in terms of mesh size. In the current simulations, mesh size of 5mm was assigned globally, while dense mesh was adapted in abrupt geometrical change, such as holes, to accommodate better mesh application and minimize errors due to mesh size. A validation via prototype was carried out instead to realize the validation of the FE model.

Since using cadaveric human bone may not demonstrate the same bone geometry as the bone used in the FE model. A scaled validation of the FE model was proposed to validate the geometry and mesh of the FE model. The approach started by constructing the bone geometry same as that of the FE model by a rapid prototyping machine. The bone would then be fixed with the implant components. The bone-implant complex would be mounted on a mechanical testing machine. The stress distribution and magnitude of the tibial insert would be investigated by pressure sensors, Fuji film. The boundary conditions would feedback to the environment of the FEA. For example, the material property of the bones would change to that of the prototype. The magnitude of load applied would be lower and consistent with the testing load of the mechanical testing machine. Since validation in terms of stress of the bone, as predicted in the parametric studies, is not viable, the comparison would be based on the contact pressure of the tibial insert. Once the contact pressure is validated, the computation of the finite element model is assumed to be accurate within tolerance. The variation of different parameters in the parametric studies is also regarded as validated.

3.3.1 Rapid Prototyping

The rapid prototyping machine that imported was of Fused Decomposition Modeling, marketed by Stratasys incorporated. The machine is of brand Dimension BST 768 (Breakaway Support Technology). The specifications of the prototype machine are listed on **Fig. III-10**. It makes use of a moving and heating nozzle to melt material, such as Acrylonitrile Butadiene Styrene (ABS) and spray on a particular position. The material hardens and binds together to form the geometrical layer.

Build Size	203x203x305 mm
Material	Standard ABS
Layer Thickness	0.245mm or 0.33mm

Fig. III-10 Dimension BST 768 with specifications.

Fig. III-11 shows the prototype of the femur, tibial, together with the imported implant. The purpose of the rapid prototyping is to reproduce the exact geometry as the MRI, so as to validate the finite element model.

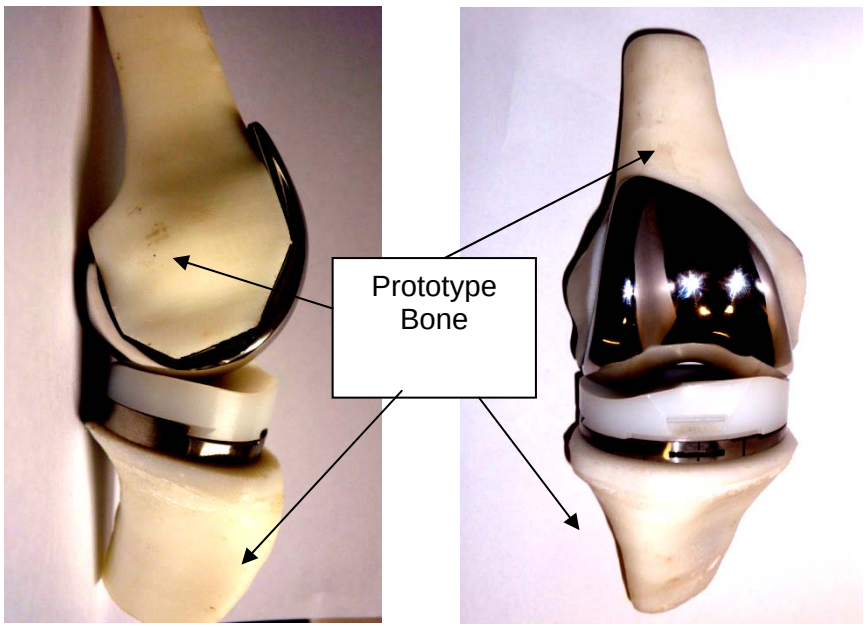

Fig. III-12 Prototype of plastic bones with the implant. Sagittal view (left), front view (right)

3.3.2 Verification of Contact Pressure

Verification of contact pressure was commonly preceded by Fuji film (Liau et al., 2001; Liau et al., 2002). Fuji film is a pressure sensing film, incorporated in the Fuji digital analysis system (**Fig. III-13**).

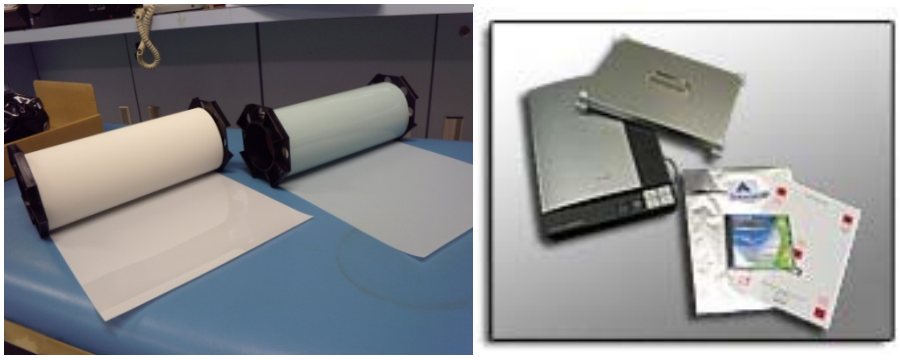

Fig. III-13 Fuji Film and Fuji Digital Analysis System for Prescale (Tekscan Inc., USA)

When pressure was applied on the Fuji film, the microcapsules were broken and the color-forming material reacted with the color-developing material to make red color (Fig. III-14). The micro-capsules are designed to break according to the pressure so the color density corresponds to the pressure. (Tekscan Inc., USA)

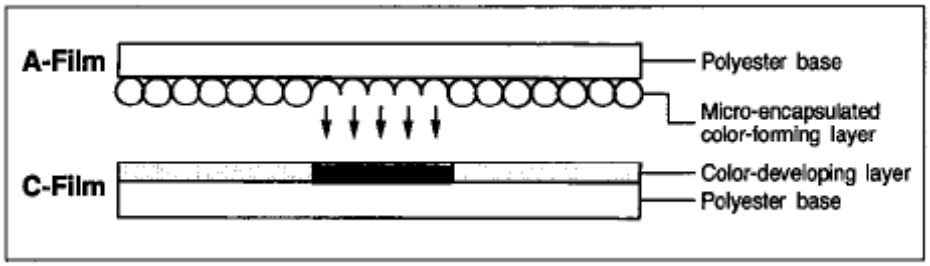

Fig. III-14 Working principle of Fuji film. (Tekscan Inc., USA)

This system could convert color density values into pressure values. The scanner of the system could improve data-read precision, together with calibration to limit scanner-read errors to a fixed range.

The common types of Fuji film used in knee implant verification includes: LLW (0.5-2.5MPa), LW (2.5-10MPa), and MS (10-50MPa). Villa et al. (2004) applied a coefficient of friction of 0.12, while Godest et al. (2002) applied 0.01, 0.04 and 0.07 coefficient of friction on the model. They produced similar results as that of Liau et al. (2002) of which preceded FEA with Fuji film experiments.

Liau et al. (2001, 2002) also preceded study of Fuji film to investigate the effect of

using different types of Fuji film and they discovered that LW-type overestimated knee implant actual contact area by 1.2-2.4% and MS-type underestimated actual contact pressure by 8-14%.

The calibration process was preceded with the aided of the calibration curve provide by the Fuji film manufacturer. **Fig. III-15** shows the calibration curve of Fuji film.

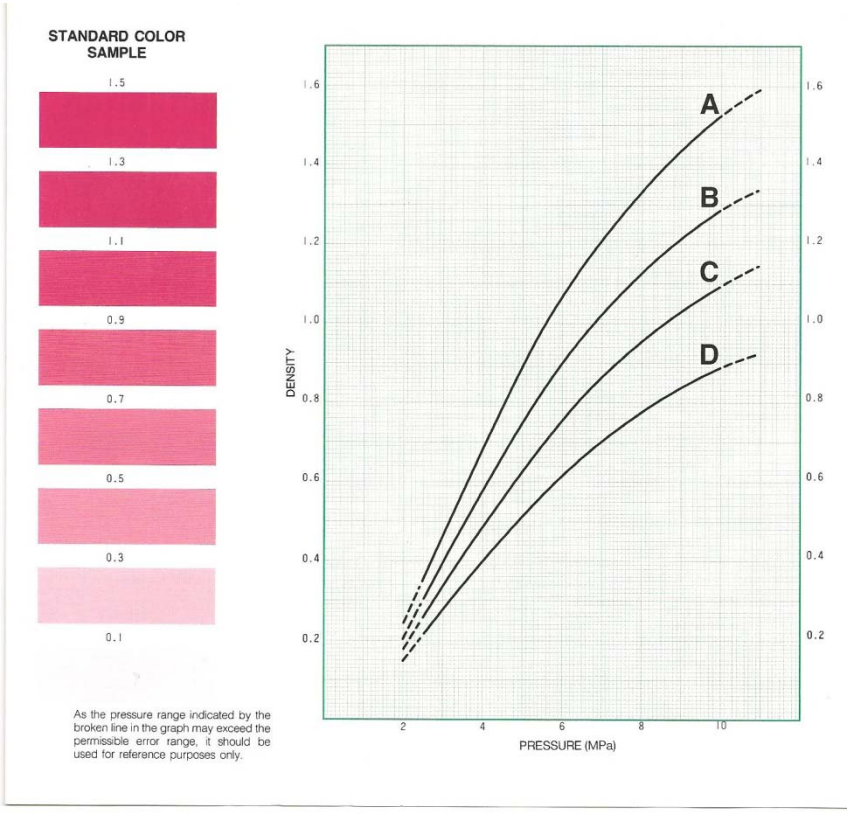

Fig. III-15 Calibration curve of Fuji film, showing the relationship between color density to applied pressure, provided by the manual of the product.

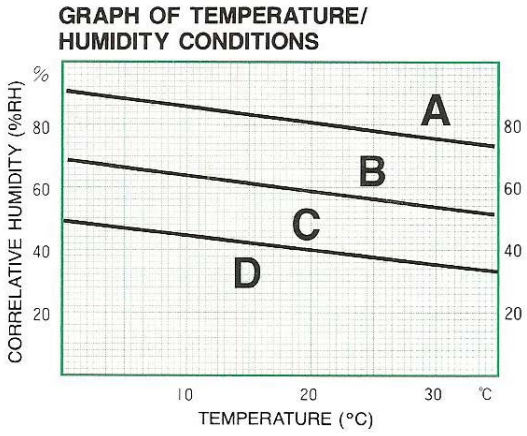

Fig. III-16 Calibration graph based on temperature and humidity conditions,

provided by the manual of the product

The room temperature in the laboratory was about 20 degree Celsius and the humidity was about 60%RH. Curve C was chosen as the calibration curve (**Fig. III-16**). Since the definition of color density was not clear, the density value was converted into color value in photo-processing software. Respective color density of 1.5 was valued 197, whereas that of 0.1 was valued 51.

CHAPTER IV RESULTS

4.1 Effects of Varying Compressive Loading

Fig. IV-1 shows the relationship of contact pressure of tibial insert to the applied loading and flexion angle. Since 2000N compressive force was regarded as the reference of load application. The compressive load was normalized using 2000N. At 100% loading (2000N), the minimum predicted contact stress was 23.28MPa at 30-degree, while the maximum predicted contact stress was 25.68MPa at 60-degree.

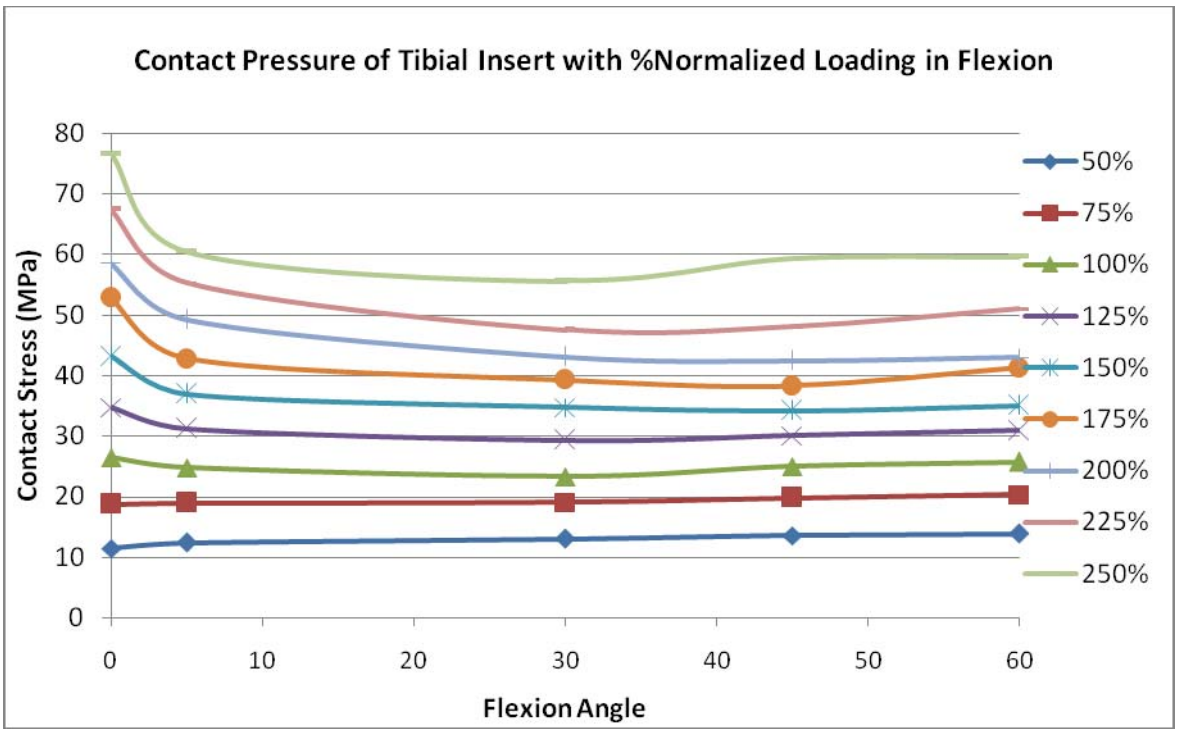

Fig. IV-1 Predicted contact pressure of tibial insert with %normalized loading in flexion.
The line indicated 100% represented compressive load of 2000N, while the other percentage represented the multiples to 2000N compressive load.

The predicted contact stress of the tibial insert was sensitive to the applied load of the implant. Average 23% increase of contact stress would be resulted with an increase of 25% applied load. This indicated that a person with higher weight could result in higher stress on the tibial insert, or a fall could easily impose high stress on the implant.

Upon the shear of femur, the maximum principal shear of the cortical femur increased from about 1.5MPa at 5-degree to 6.4MPa at 60-degree (**Fig. IV-2**).

The minimum shear decreased by 47% and the maximum shear decreased by 63% when the applied loading decreased by 50%. The maximum and minimum shear increased by 100% when the applied force increased by 100%.

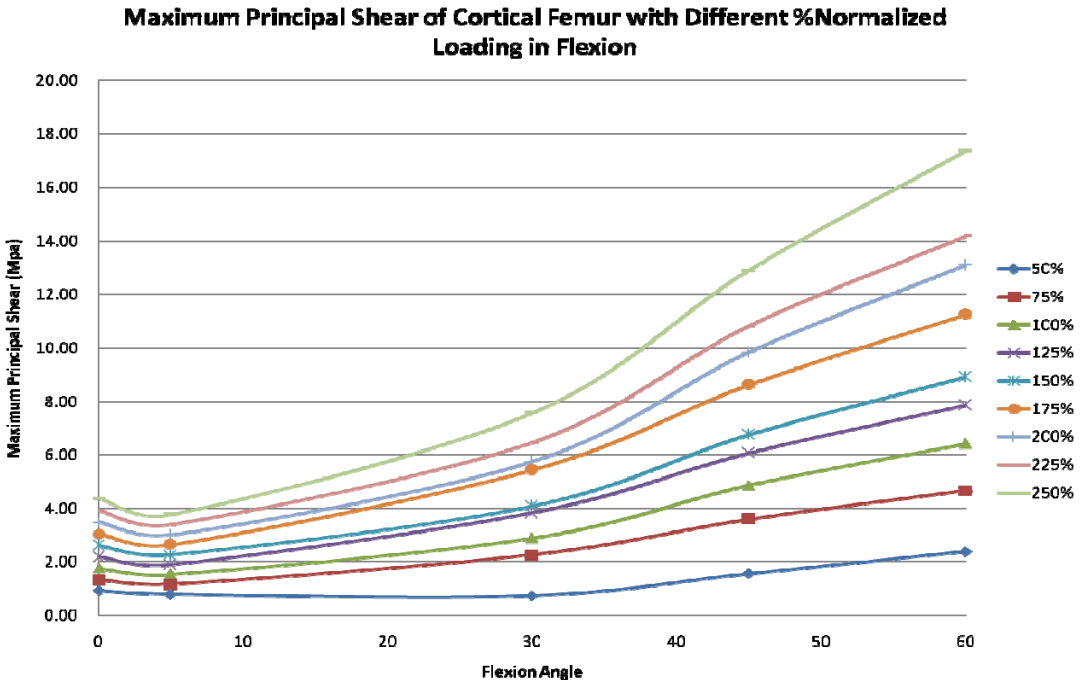

Fig. IV-2 Maximum principal shear of cortical femur with different %normalized force loading in flexion
The line indicated 100% represented compressive load of 2000N, while the other percentage represented the multiples to 2000N compressive load.

The maximal principal shear of the trabecular increased from about 0.288MPa at 5-degree to 0.475MPa at 60-degree (**Fig. IV-3**). The minimum shear decreased by 49% and the maximum shear decreased by 53% when applied loading decrease by 50%. The minimum shear increased by 98.5% and the maximum shear increased by 103%.

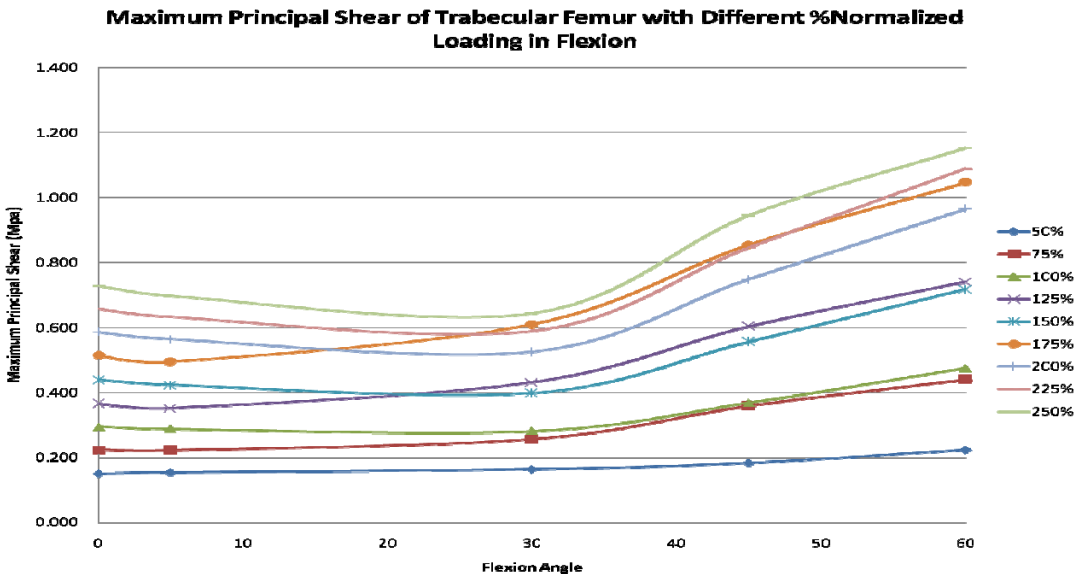

Fig. IV-3 Maximum principal shear of trabecular femur with different %normalized force loading in flexion
The line indicated 100% represented compressive load of 2000N, while the other percentage represented the multiples to 2000N compressive load.

4.2 Effects of Varying Trabecular Bone Stiffness

Fig. IV-4 shows the results of predicted contact pressure of tibial insert with percentage normalized trabecular bone stiffness. An elastic modulus of 389MPa in femur (Rohlmann et al., 1980) and 445MPa in tibia (Linde et al., 1989) indicated 100% bone stiffness.

The predicted FE results showed that stronger trabecular bone stiffness could reduce the contact stress of the tibial insert slightly. In fact, the sensitivity of flexion angle outweighed that of trabecular bone stiffness.

With respect to the effect on bone, due to the strength of cortical bone, most of the stress was born by the cortical bone. The stress of cortical femur increased from 20MPa at 5-degree to 59MPa at 60-degree at 100% loading. The minimum and maximum stress increased by 3.5% and 7.2% respectively, when the bone strength was reduced by half, while the minimum and maximum stress decreased by 5% and 18.5% when the bone strength was increased by 100% (**Fig. IV-5**). The stress of trabecular femur increased from 1.39MPa at 5-degree to 3.96MPa at 60-degree. The minimum and maximum stress increased by 3.87% and 2.94% respectively, when the bone strength was reduced by half, while the minimum and maximum stress increased by 6.60% and 2.31% when the bone strength was increased by 100% (**Fig. IV-6**).

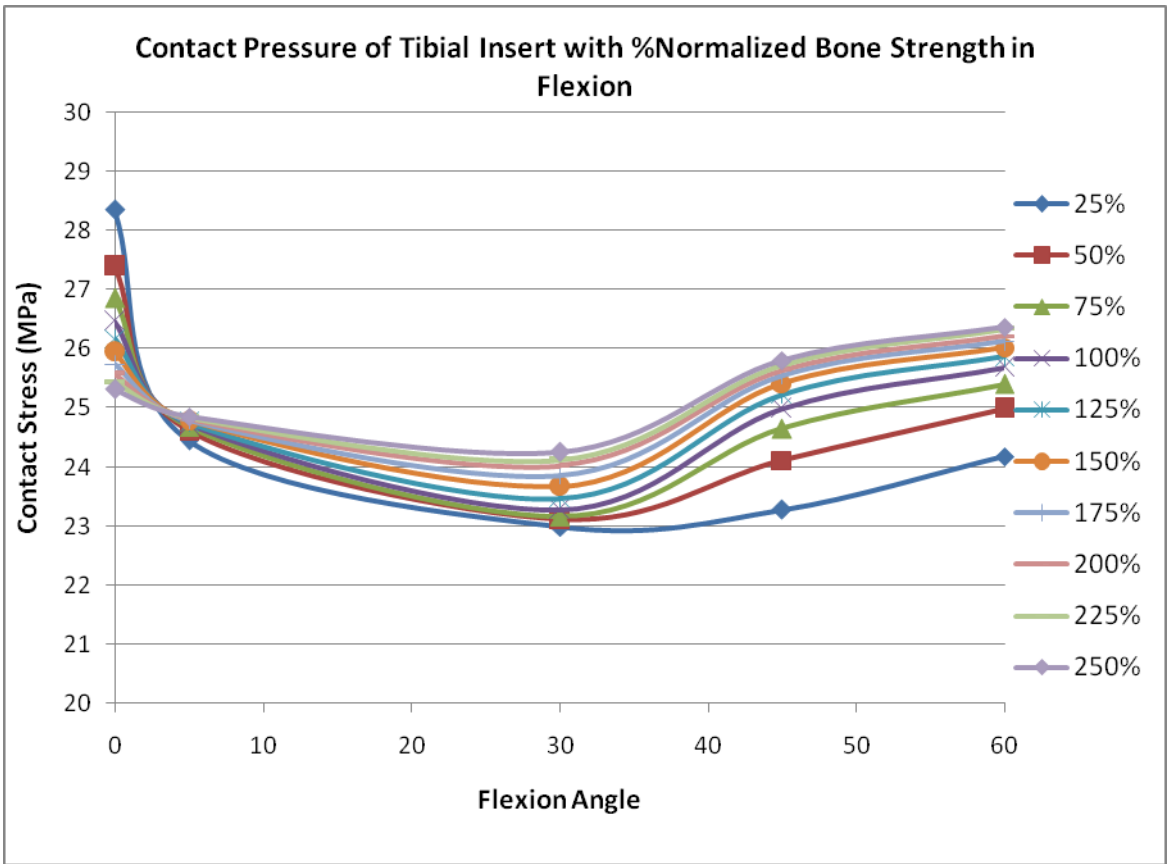

Fig. IV-4 Predicted contact pressure of tibial insert with %normalized bone strength in flexion
The line indicated 100% represented trabecular bone stiffness of 389MPa in femur and 445MPa in tibia, while the other percentage represented the multiples to these values of bone stiffness to femur and tibia respectively.

Due to the vulnerability of stress peak at the posterior supra-condylar region of trabecular femur, the von Mises stress was extracted out for analysis. The stress value of the trabecular femur at lower flexion angle was corresponding to that of posterior supra-condylar region, of which representing peak stress occurred at this region while lower flexion angle (**Fig. IV-7**).

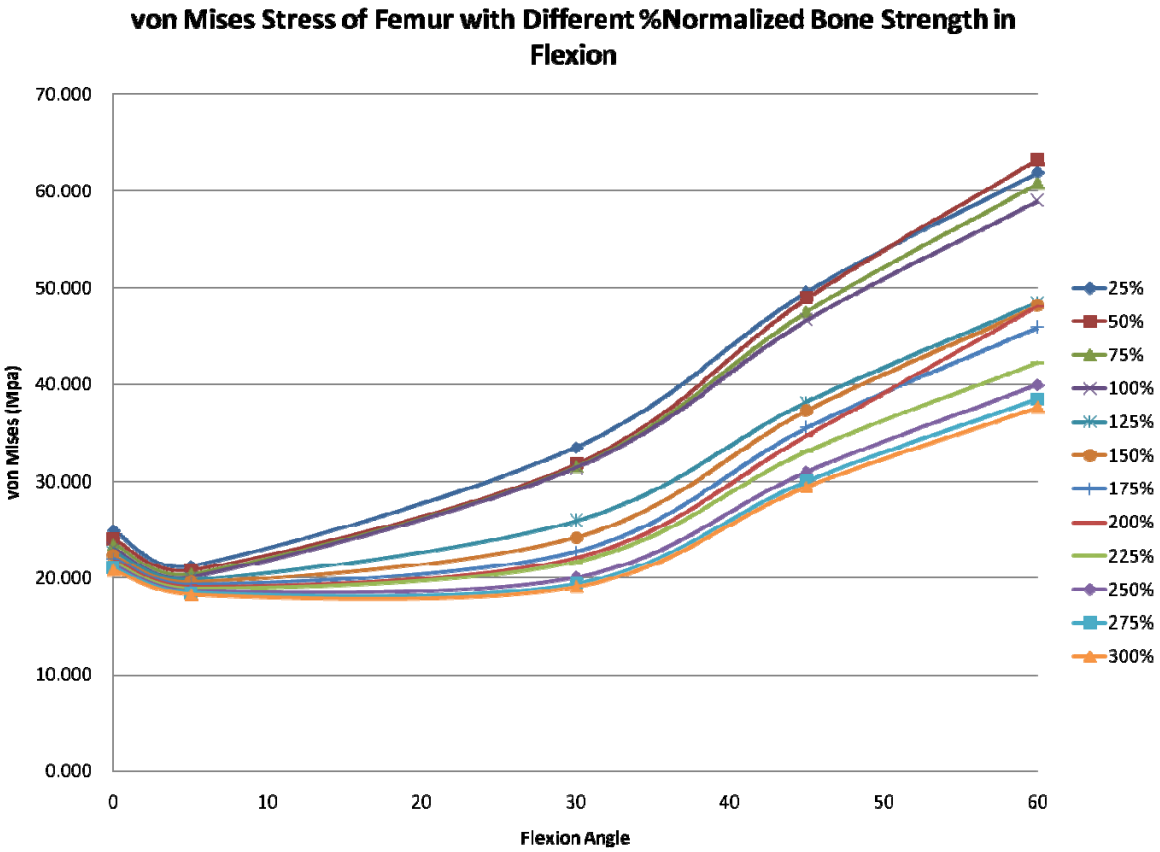

Fig. IV-5 Predicted von Mises Stress of cortical femur with different %normalized bone strength in flexion

The line indicated 100% represented trabecular bone stiffness of 389MPa in femur and 445MPa in tibia, while the other percentage represented the multiples to these values of bone stiffness to femur and tibia respectively.

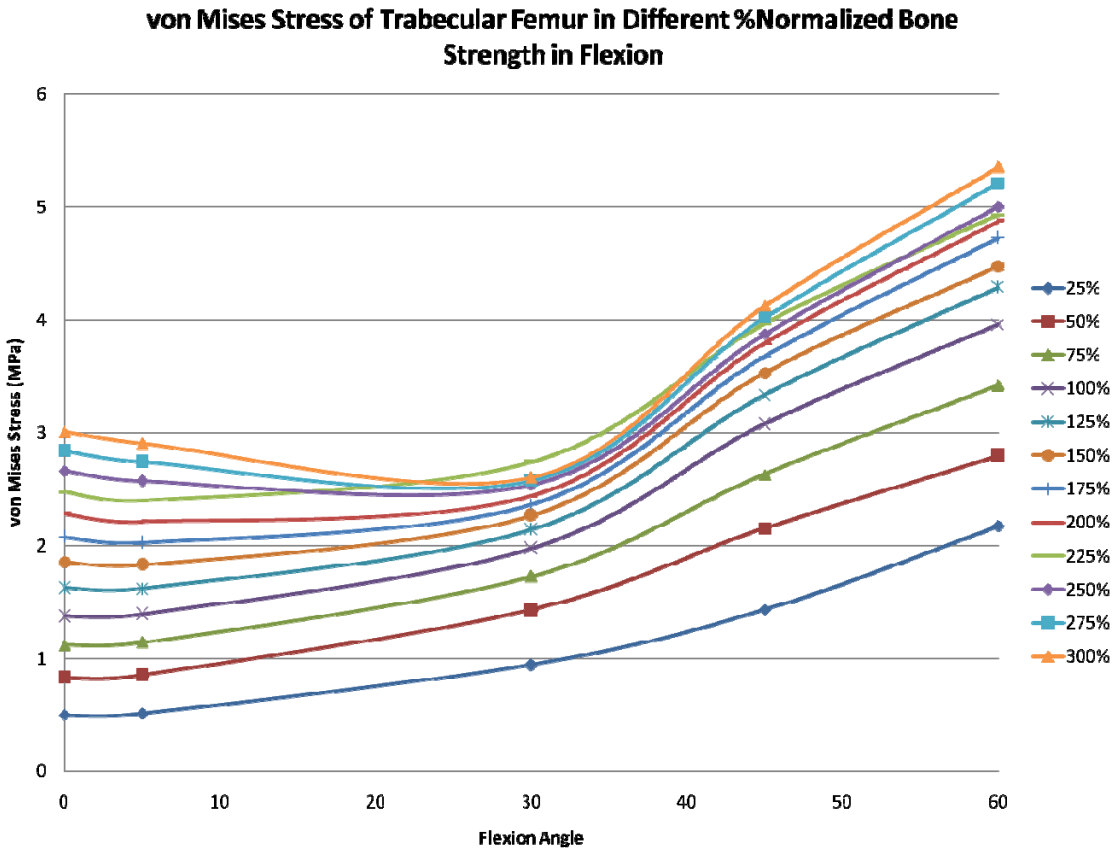

Fig. IV-6 Predicted von Mises of trabecular femur in different %normalized bone strength in flexion.
The line indicated 100% represented trabecular bone stiffness of 389MPa in femur and 445MPa in tibia, while the other percentage represented the multiples to these values of bone stiffness to femur and tibia respectively.

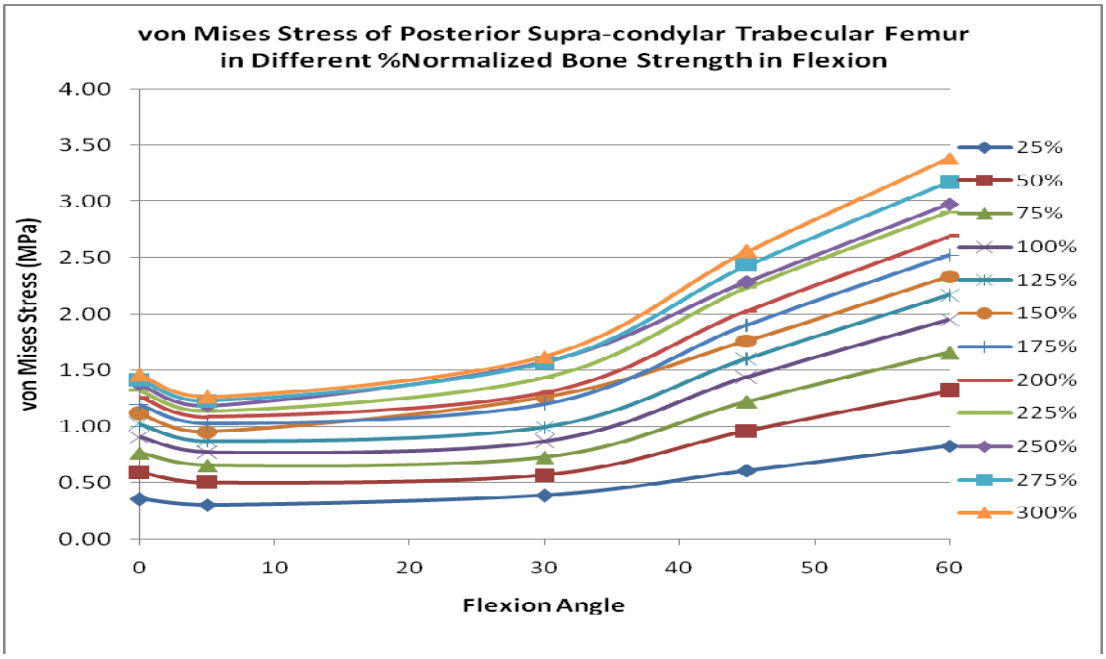

Fig. IV-7 Predicted von Mises stress of posterior supra-condylar trabecular femur in different %normalized bone strength in flexion
The line indicated 100% represented trabecular bone stiffness of 389MPa in

femur and 445MPa in tibia, while the other percentage represented the multiples to these values of bone stiffness to femur and tibia respectively.

4.3 Effects of Flexion Angle

Upon the effect on the contact stress of the tibial insert, the contact stress increased with flexion angle. However, the increase was not very sensitive. The difference between the highest and lowest stress value in different flexion angles was about 6%.

Fig. IV-4 shows a predicted contact stress pattern to the flexion angle, at different loading. The predicted contact stress was larger from neutral to 5-degree and gradually reduced to flexion 30 degrees. Then, It increased until 60-degree. This result was different from that of Chu in 1999. Chu discovered that the contact area decreased from area contact to line contact, with increasing flexion angle. The difference might be due to the specific implant model in different predictions. In this FE prediction, the predicted contact stress was larger at neutral position compared with the results from 5-degree flexion to 30-degree flexion. However, the implant might be at a locking stage or with certain degree of hyper-extension to keep the knee stable. This might reflect the reason of high stress at neutral position. The stress became lower from 0-degree to 30-degree flexion, which was a common flexion range in walking. The stress increased again from 30-degree flexion to 60-degere flexion due to reduction in contact area. Shuichi et al. (1998) conducted an experiment using K-Scan and Instron servo-hydraulic testing device. They showed that contact stress increased gradually with increased flexion. In order to verify the comparison, contact area in different flexion angles could be extracted to verify different models.

4.4 Simulation of Gait Condition

Gait simulations were also carried out based on boundary conditions of ISO-14243-3. **Fig. IV-8** shows the compressive force applied in different instance of gait cycle. **Fig. IV-9** shows the steps of the FE simulating gait.

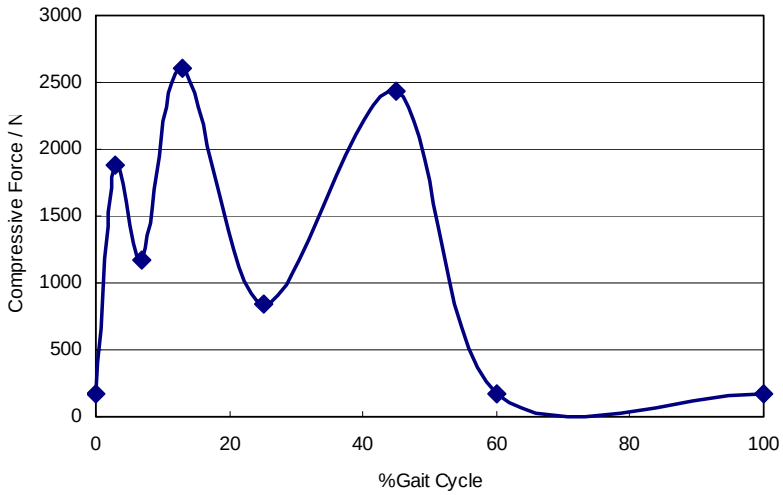

Fig. IV-8 Compressive force in simulating gait in different instance (ISO-14243-3)

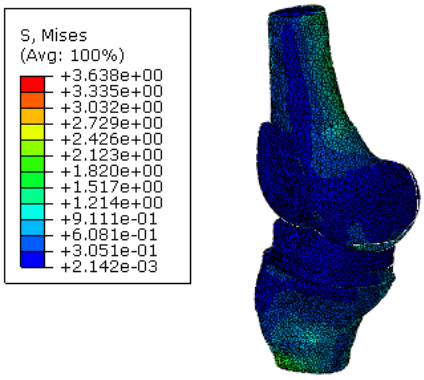

Phase A, Gait Cycle:0%,
Flexion angle 0 degree

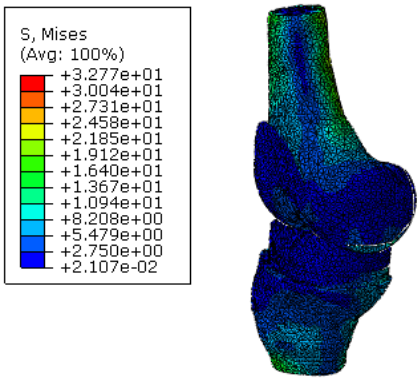

Phase B, Gait Cycle:3%,
Flexion angle 1.53 degree

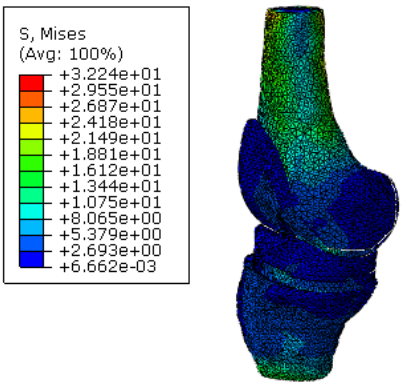

Phase C, Gait Cycle:7%,
Flexion angle 7.16 degree

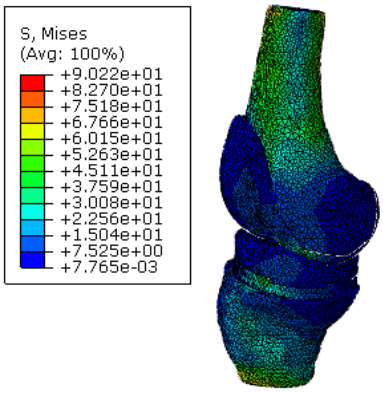

Phase D, Gait Cycle:13%,
Flexion angle 15.13 degree

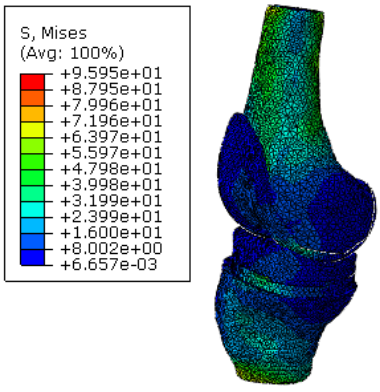

Phase E, Gait Cycle:16%,
Flexion angle 15.96 degree

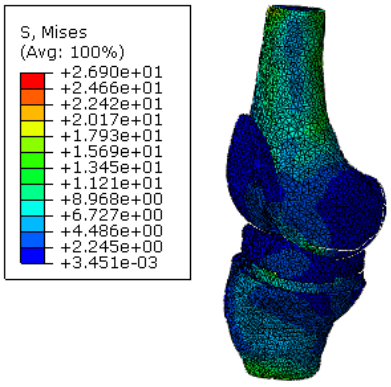

Phase F, Gait Cycle:25%,
Flexion angle 12.25 degree

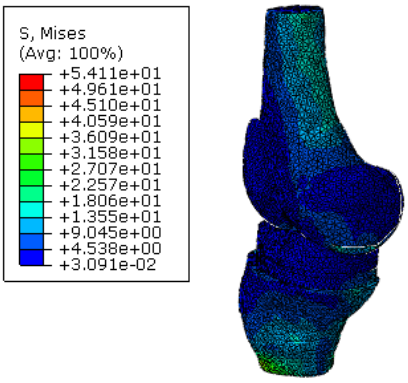

Phase G, Gait Cycle:41%,
Flexion angle 5.13 degree

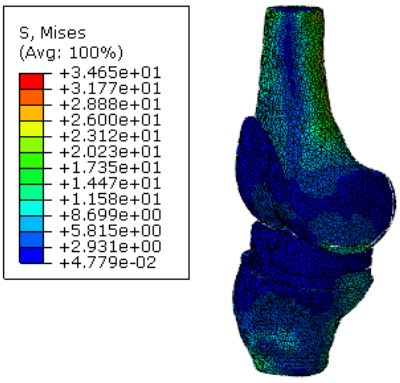

Phase H, Gait Cycle:45%,
Flexion angle 8.13 degree

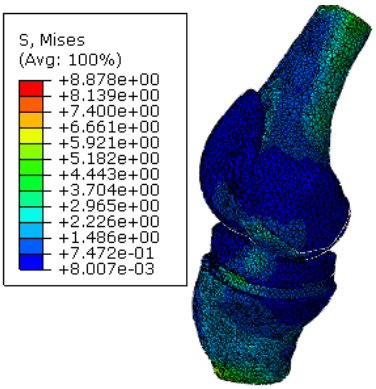

Phase I, Gait Cycle:60%,
Flexion angle 41.64 degree

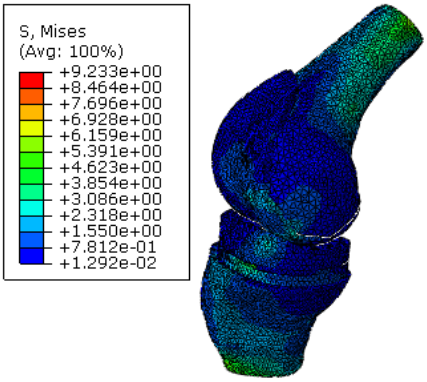

Phase J, Gait Cycle:73%,
Flexion angle 57.82 degree

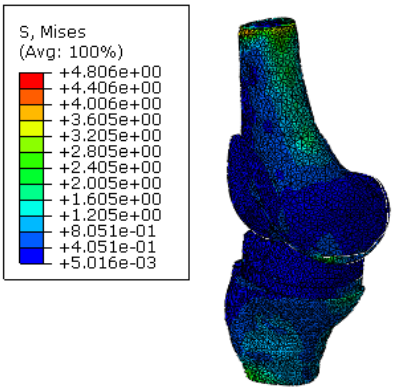

Phase K, Gait Cycle:100%,
Flexion angle 0 degree

Fig. IV-9 Predicted FE results of different steps in simulations on gait

The predicted contact pressure of the tibial insert was plotted against the percentage gait cycle (**Fig. IV-10**).

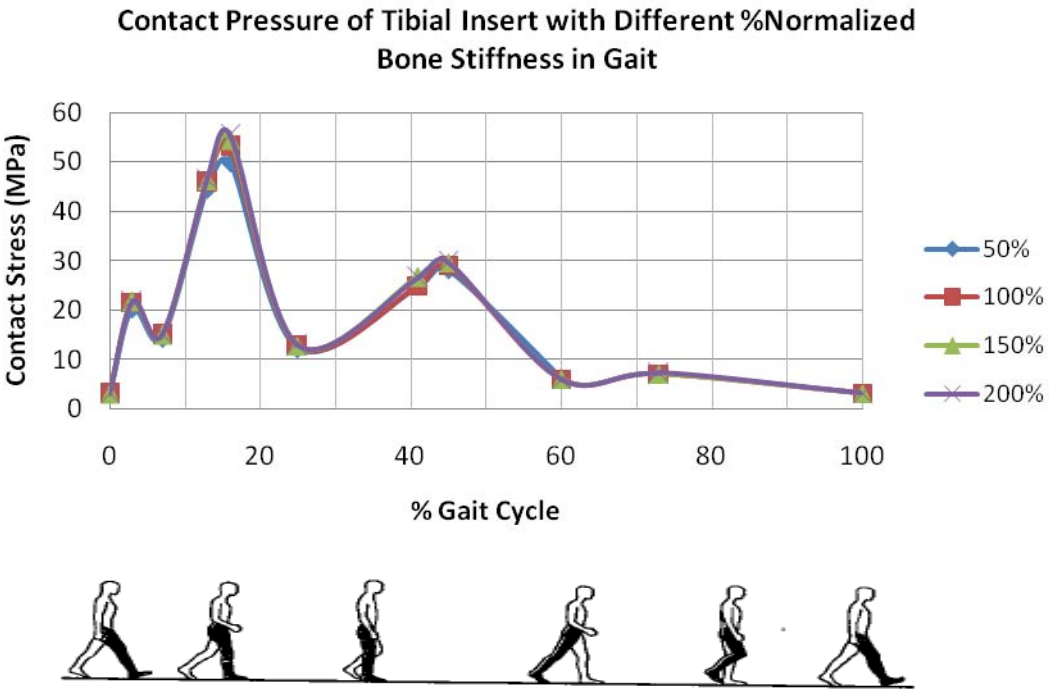

Fig. IV-10 Predicted contact pressure of tibial insert with different %normalized bone stiffness in gait.
The line indicated 100% represented trabecular bone stiffness of 389MPa in femur and 445MPa in tibia, while the other percentage represented the multiples to these values of bone stiffness to femur and tibia respectively.

The predicted contact stress of tibial insert upon gait had two peaks at 16% gait cycle and 45% gait cycle. These two peaks corresponded to two high compressive forces at these two instances. At 16% gait cycle, the predicted contact stress reached 53MPa. At 45% gait cycle, the predicted contact stress reached 29MPa.

Figure 4-5 shows the stress distribution along the gait and also around the instance of 16% gait cycle. The stress distribution was concentrated at the two condylar regions (**Fig. IV-11**).

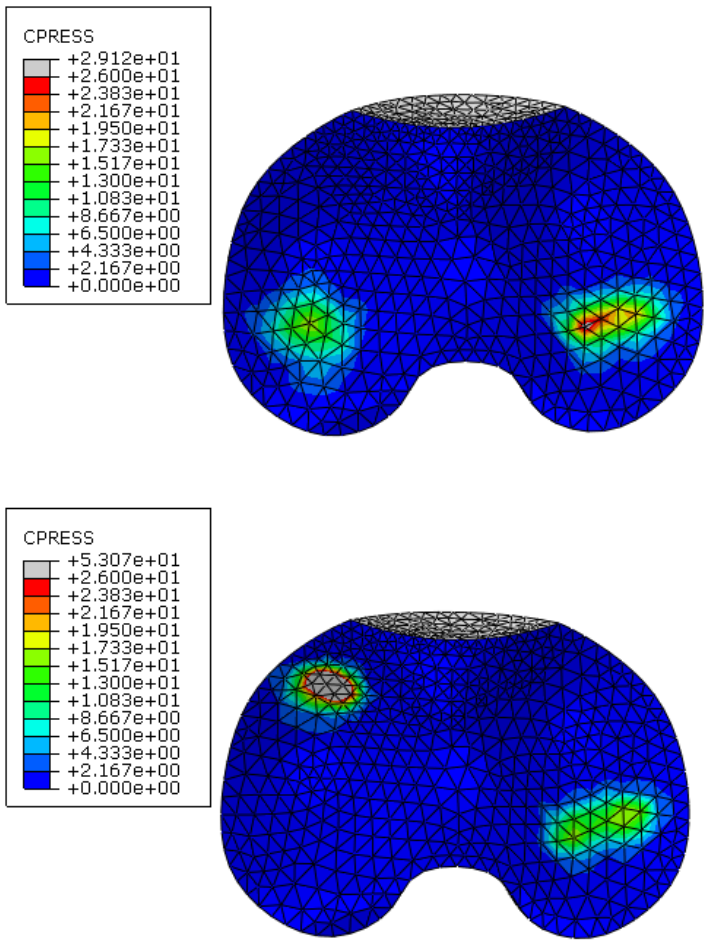

Fig. IV-11 Stress distribution of tibial insert: normal stress distribution at the bicondylar region (up), stress shifts anteriorly at 16% gait cycle (down)

CHAPTER V DISCUSSIONS

5.1 Contact Pressure of Tibial Insert

5.1.1 Static Condition

The contact stress between the femoral component and the tibial insert refers to the stress experienced at the surface of the tibial insert upon the touching to the femoral component, one or more points. The contact stress of the tibial insert affects the probability of wear of the knee replacement, and thus its longevity. Therefore, the analysis of tibial insert contact stress is necessary to judge the success of an implant design. Most of the existing FEA carried out an investigation on the contact stress of tibial component.

At 100% loading (2000N), the predicted minimum contact stress was 23.28MPa at 30-degree, while the predicted maximum contact stress was 25.68MPa at 60-degree. The results were comparable to that of existing FE literatures, ranged from about 17MPa to 27 MPa. A mechanical testing experiment carried out by Shuichi et al. (1998) showed a contact stress of about 15MPa at neutral position and about 40MPa at 60-degree flexion at about 3300 N compressive force. Bristol et al. (1994) tested eight kinds of implants using pressure sensors at 2775N load with 60-degree flexion. Contact stress of about 25MPa showed the highest engagement in their histogram study. In fact, the predicted FE stress has not reached the 27MPa yield strength of the UHMWPE (Chu, 1999). However, even half the load, the predicted contact stress still exceeded the suggested allowable stress of 10MPa of the UHMWPE (Chu, 1999).

The predicted contact stress of the tibial insert was sensitive to the applied load of the implant (**Fig. IV-4**). Average 23% increase of contact stress would be resulted in an increase of 25% applied load. This indicates that a person with higher weight could result in higher stress on the tibial insert, or a fall could easily impose high stress on the implant. The contact stress increased with flexion angle. However, the increase was not very sensitive. The difference between the highest and lowest stress value in different flexion angles was about 6%. Since, greater flexion would reduce the contact area of the implants and increase the contact stress (Chu, 1999). Insensitive stress level upon presumed flexion range may indicate a better knee implant design in maintaining contact area in different flexion angles.

The predicted FE results showed that stronger trabecular bone stiffness could

reduce the contact stress of the tibial insert slightly (**Fig. IV-6**). In fact, the sensitivity of flexion angle outweighed that of trabecular bone stiffness. The FE prediction suggested that osteoporotic patients may not affect the wear and durability of the tibial component. Further observation and experiment should be done to prove this hypothesis.

Fig. IV-4 shows a contact stress pattern to the flexion angle, at different loading. The contact stress was larger from neutral to 5-degree and gradually reduced to 30-degree of flexion. Then, It increased until 60-degree. This result was different from that of Chu in 1999. Chu discovered that the contact area decreased from area contact to line contact, with increasing flexion angle. The difference may due to the specific implant model in different prediction. In current FE prediction, the contact stress was larger at neutral position compared with the results from 5-degree flexion to 30-degree flexion. However, the implant may be at a locking stage or with certain degree of hyper-extension to keep the knee stable. This may reflect the reason of high stress at neutral position. The stress became lower from 0-degree to 30-degree flexion, which was a common flexion range in walking. The stress increased again from 30-degree flexion to 60-degere flexion due to reduction in contact area. Shuichi et al. (1998) conducted an experiment using K-Scan and Instron servo-hydraulic testing device. They showed that contact stress increased gradually with increased flexion. In order to verify the comparison, contact area in different flexion angles should be extracted to verify different models.

5.1.2 Gait Condition

Gait simulations were also carried out based on boundary conditions of ISO-14243-3. The predicted contact stress of tibial insert upon gait had two peaks at 16% gait cycle and 45% gait cycle. These two peaks corresponded to two high compressive forces at these two instances. At 16% gait cycle, the predicted contact stress reached 53MPa. At 45% gait cycle, the predicted contact stress reached 29MPa. Compared with existing literatures, Chu (1999) found a maximum compressive stress of 17.2MPa at 55% of gait cycle, while Halloran et al. (2005) discovered a maximum compressive stress of about 20MPa at 45%-55% of gait. The peak at 45% gait cycle could correspond to the results of these two literatures (Chu, 1999; Halloran et al., 2005).

Fig. IV-10 shows the stress distribution along the gait and also around the instance of 16% gait cycle. The stress distribution was concentrated at the two

condylar regions (**Fig. IV-11**), which was comparable to the FE predictions of Georgeanu and Gruionu (2006) (**Fig. V-1**). When the step reached around 16% gait cycle, the stress of medial side shifted anteriorly abnormally (**Fig. IV-11**). In fact, a lot of existing knee implant designs were symmetrical. However, this implant was asymmetrical medial pivoting design, allowing tibial rotation upon flexion. The boundary conditions of gait may be over-constrained with the implant's rotation and leading to extra peak stress. Since different implant designs could present different knee kinematics, such as anatomical and functional. A universal boundary condition for gait simulation may not be appropriate in comparing stress between different implant designs.

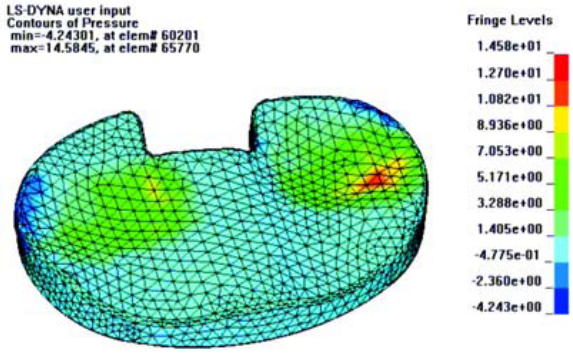

Fig. V-1 Stress contour in FE prediction of Georgeanu and Gruionu (2006).

5.2 Investigation on Periprosthetic Fracture

Periprosthetic fracture was one of the causes of failure with prevalence ranged from 0.3 to 2.5% and 1.6 to 38% after revision surgery (Edward et al., 2004). Though uncommon, complications of post-periprosthetic fracture were devastating and rates from 25 to 75% were reported (Douglas et al., 2001). A majority of the fracture is associated with elderly patients with osteoporosis and rheumatoid arthritis patients receiving steroid therapy. These risk factors are related to the reduction of bone stock, thus bone strength and results in stress alteration of bone. Understanding the association and mechanism can aid physicians to decide viable knee replacement.

In this study, the periprosthetic fracture would be investigated in three aspects. Firstly, the von Mises stress alteration due to bone stiffness reduction would be discussed. It is then followed by the study of maximum principal shear and strain. The results would then be compared to respective yielding value to determine the risk of fracture.

From the stress contoured of FE, the stress of the femur concentrated on three locations: apex of screw-hole, anterior flange location, and posterior

supra-condylar location (**Fig. V-2**). These three points linked to be the fracture line which correlated with clinical finding (**Fig. V-3**). The fracture regions also related to flexion, as the concentrated stress shifted upon flexion (**Fig. V-4**).

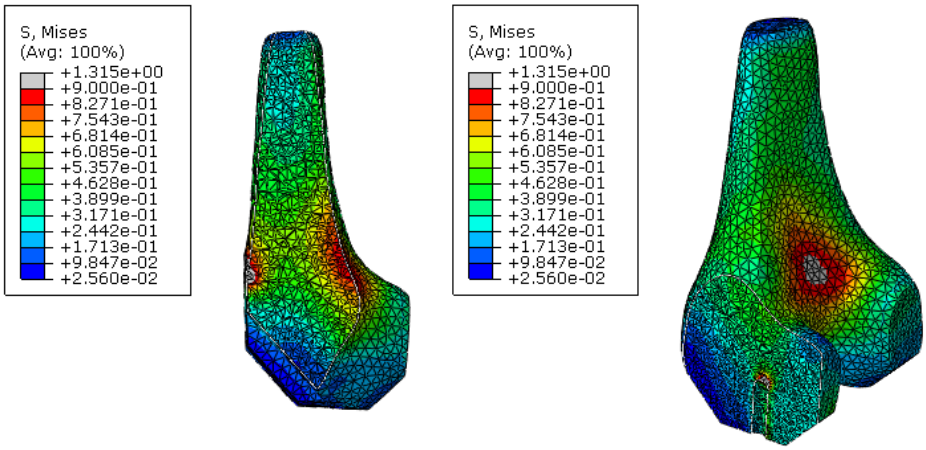

Fig. V-2 Concentrated stress on femur at anterior flange, apex of screw hole and posterior supra-condylar location.

Fig. V-3 Periprosthetic fracture location taken from X-ray: sagittal view (right) frontal view (left) (Han et al., 2009).

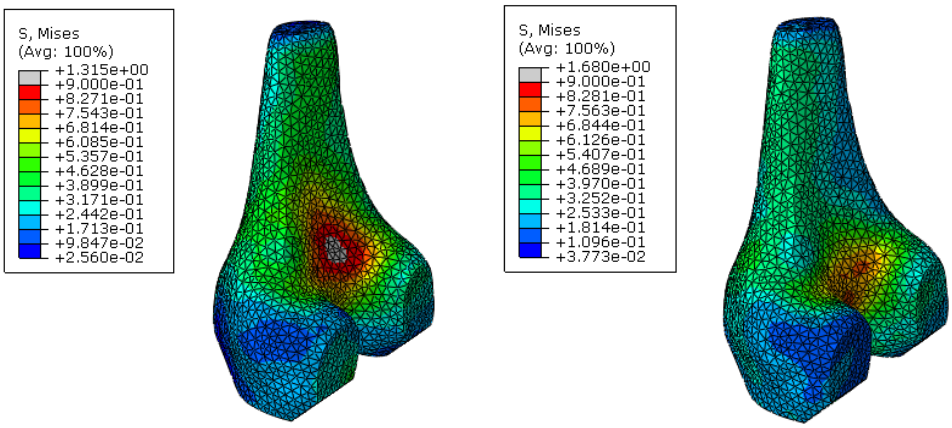

Fig. V-4 Shift of concentrated stress at different phrase of gait with different flexion angle.

However, the peak von Mises stress location changed with flexion angle. In lower flexion angle, the stress concentrated on the posterior supra-condylar femur region, or the screw apex region, while the stress would concentrate on the anterior flange region at a higher flexion angle. Some researchers suggested that the anterior flange region of the implant could affect the performance of implant. Indeed, the effect was more apparent on higher flexion angle, shown in this prediction.

The von Mises stress of posterior supra-condylar trabecular femur was slightly lower than the value of apex of screw. However, this region is more vulnerable to impact and onset the periprosthetic fracture.

Tissahkt et al. (1996) carried out a FEA to study the stress of distal femur after TKR. They applied 900N of tibiofemoral and 450N of patellofemoral joint reaction force. They discovered peak principal stress of 0.2MPa at the posterior condyles and 0.1MPa at the anterior distal regions (**Fig. V-5**). The stress distribution of Tissahkt et al. was comparable to the current FEA. The differences in magnitude could be due to the differences in loading magnitude and location.

Fig. V-5 Distributions of principal stress by the FE prediction of Tissahkt et al.(1996): sagittal view (left), transverse section view at interior base surface of the implant (center), transverse section view at the level of stem end (right).

Travis et al. (2009) constructed a FE model, validated by in-vitro experiment. A compressive load of 890N was applied to the model via a modeled yoke on the implant. Peak pressures of 14.4MPa, 5.0MPa and 16.5MPa were reported by three different kinds of implant (**Fig. V-6**). The peak pressure occurred at the edge of the bone-implant contact surface. From the results of the current FE prediction, the peak von Mises stress of cortical bone at 0-degree flexion to 30-degree flexion was about 20MPa. The difference in stress might be due to the difference in load application method, as well as the magnitude of bone stiffness. Travis et al. (2009) made use of a power-law relationship to approximate the bone stiffness by bone apparent density.

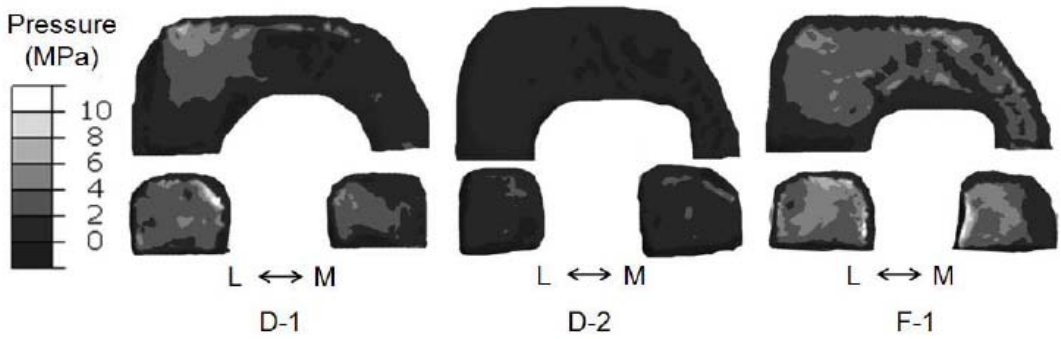

Fig. V-6 Contact pressure map of bone-implant interface surface by the FE prediction of Travis et al. (2009), D-1, D-2 and F-1 denotes different kinds of implant.

The predicted maximum principal stress in the trabecular femur was plotted against the BMAD that converted from bone stiffness, as shown in **Fig. V-7**. The two reported yield stress of trabecular specimens extracted from cadaveric knee with press-fit implant (Travis et al., 2000) was included for comparisons. Reduction of trabecular bone stress was predicted with reducing BMAD.

For a high BMAD, the predicted maximum principal stress was far from the range of yield stress of the bone. This showed that fracture was unlikely for high bone density. According to the extrapolated curve, the difference between the predicted maximum principal stress and yield stress became smaller with reduced BMAD and started to overlap with BMAD of about 0.02 g/cm3, showing a high risk of fracture. In fact, the predicted maximum principal stress would be expected to be much higher during a fall or impact condition and thus an even higher risk of fracture.

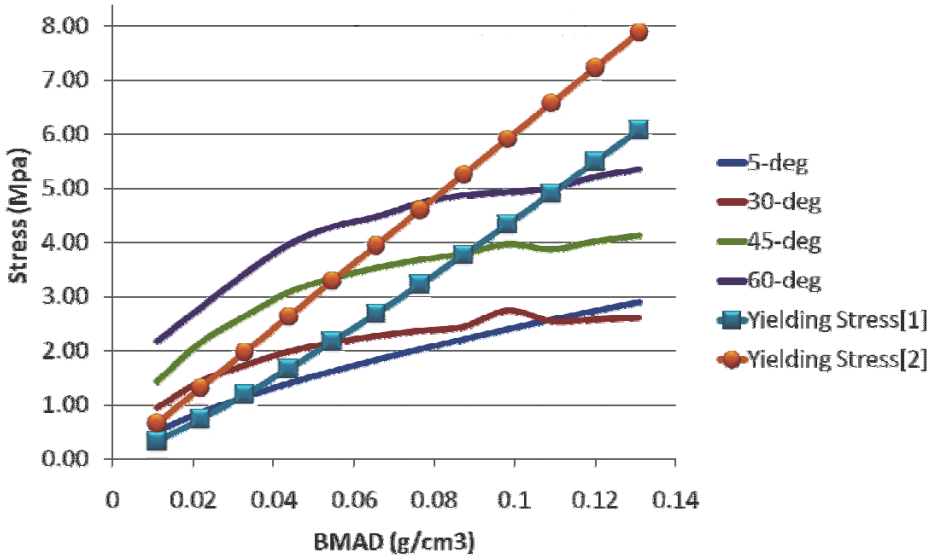

Fig. V-7 Predicted maximum principal stress against BMAD (Travis et al., 2000)

According to previous literature, the shear strength and compressive strength limit of cortical were 67MPa and 205MPa (Reilly & Burstein, 1975), of which fracture was less likely compared with that of trabecular bone. However, since trabecular bone was highly related to bone density (Ciarelli et al., 1991) and the effect of reducing strength limit outweighed that of reduced stress. At high loading, the principal shear and compressive stress exceeded the strength limit. This may lead to possible risk of fracture demonstrated at higher loading, such as impact or fall, and higher flexion angle.

Fig. V-8 shows the relationship of maximum principal strain to BMAD of trabecular femur. Principal strain reached about 1.9% at about 0.01 BMAD and 60-degree flexion, while BMAD of 0.05 at neutral position had a principal strain of about 0.02%. It was shown that high strain was contributed by low BMAD and high flexion angle. Since the reported yielding strain of trabecular bone was 0.84% (David and Tony, 1998) and the yielding strain of the bone was weakly correlated to the bone density (Koppedahl & Keaveny, 1998; Kopperdahl et al., 2002), strain failure was suggested for patients with BMAD lower than 0.02 at high flexion angle.

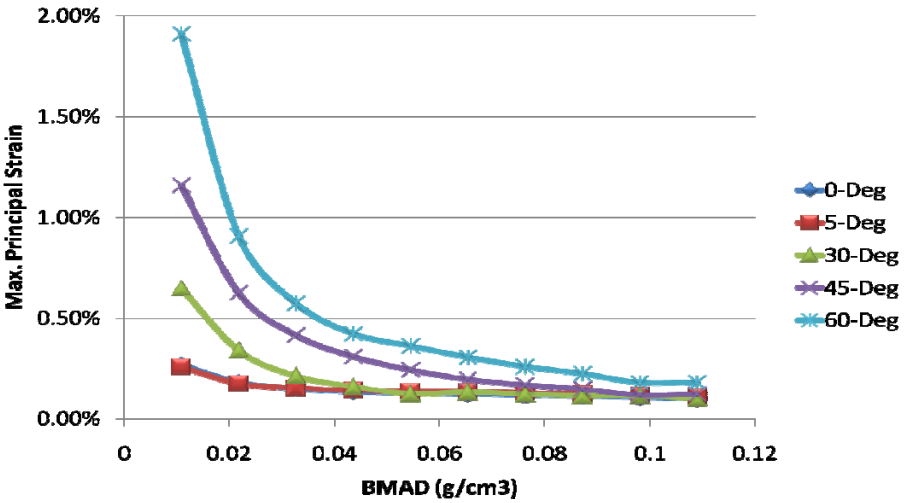

Fig. V-8 Predicted maximum principal strain against BMAD in different flexion angle.

In fact, there were few in-vitro experiments to monitor the strain of the bone. Travis et al. (2009) conducted a FEA and in-vitro experiments and installed strain gauges on the implant at the bone-implant interface. Strain of about 0.025% - 0.027% was found in their in-vitro experiment and FE simulations. Since Travis and his colleagues (2009) attached strain gauges on the implant surface at the bone-implant interface. The results were also confined to the anterior-medial and anterior-lateral regions. Further experiment should be made to verify the current FEA.

5.3 Effect of Trabecular Stiffness on Stress Shielding

Quite a number of implant-users were elderly with osteoporosis or rheumatoid arthritis patients receiving steroid therapy. Pre-existing osteoporosis reduced bone strength and could impose further risk on loosening and osteolysis. The effect of trabecular bone strength reduction to stress shielding was assessed to evaluate the risk of future loosening.

Stress Transfer Parameter (STP) would be the parameter representing the effectiveness of stress transfer, defined as the average von Mises stress ratio between the trabecular bone and the implant at the bone-implant interface.

Fig. V-9 shows the effect of BMAD on STP in different flexion angle. The STP increased with increasing BMAD, indicating less chance of stress shielding. An increase of 0.02 of BMAD could increase about 1% STP.

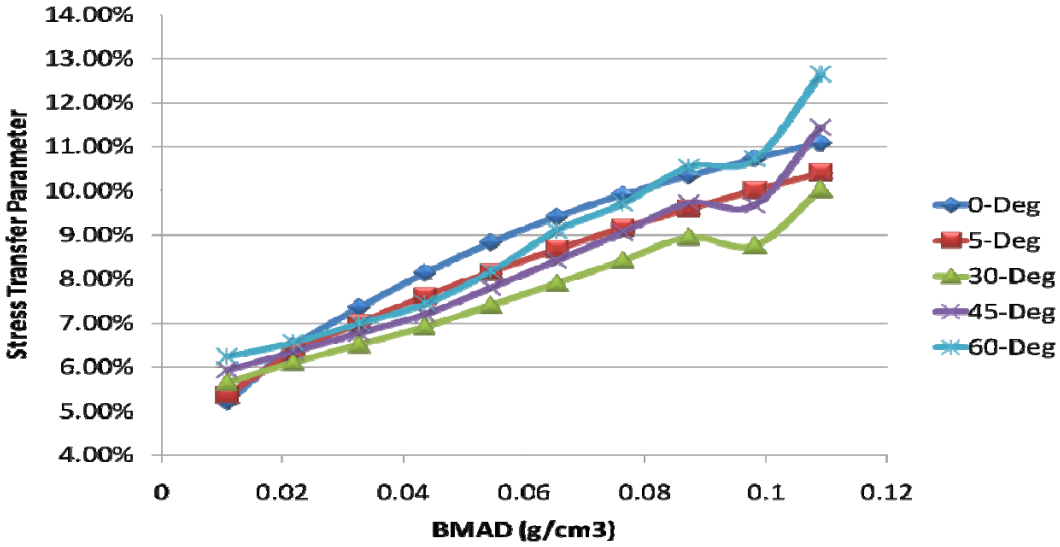

Fig. V-9 Effect of BMAD on STP in different flexion angle

The increase of BMAD indicated an increase of material stiffness of trabecular bone. The increase of stiffness resulted in higher load sharing proportion that leads to higher stress transfer capacity. The STP also increased with degree of flexion due to a higher stress at a higher flexion angle. The STP of neutral position was also abnormally higher because of higher stress due to possible locking and hyperextension of the implant.

There was different research on stress shielding of bone. Tissakht et al. (1996) constructed a FE model with 900N tibiofemoral force and 450N patellofemoral force. They defined stress shielding effect by the reduction of maximum magnitudes of strain energy density. A maximum stress shielding was 15%, occurred at the anterior distal corner of the femur. Completo et al. (2009) developed a FE model of tibial and implant tibial component, with a compressive force of 1440N medially and 880N laterally. Completo et al. (2009) defined stress shielding as the reduction of principal stress compared with that of intact bone model. A maximum stress shielding of 82% was found at the medial portion of the implant (**Fig. V-10**).

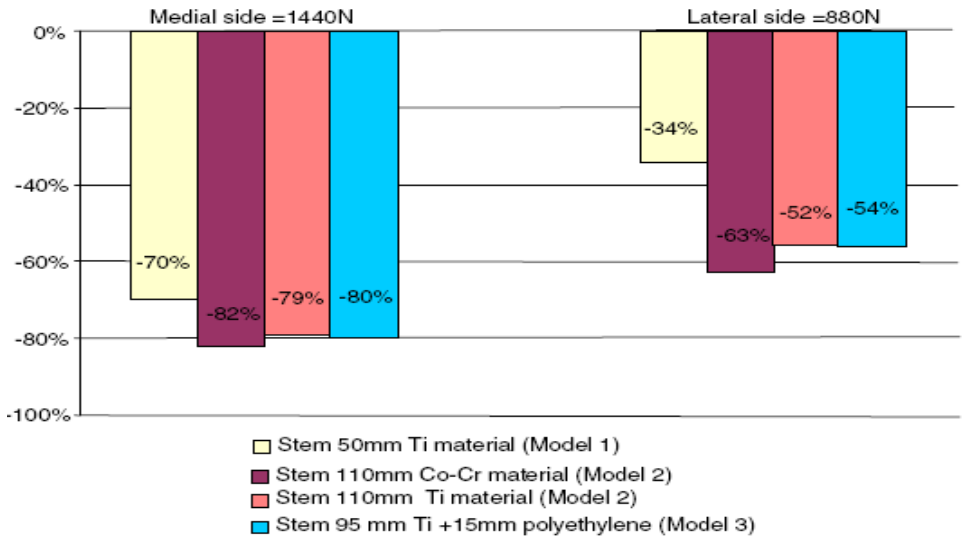

Fig. V-10 Stress shielding of medial and lateral compartment of the implanted tibia (Completo et al., 2009)

Reduction of stress shielding of 82% could correspond to the stress transfer parameter of about 6-12% in current study. Due to the large difference between bone and implant stiffness, implant took up most of the stress from the load. Stress shielding was a common problem and 70% of TKR cases experienced radiographic evidence of bone loss (Cameron & Cameron, 1987; Mintzer et al., 1990). Further experiments should be made to better quantify the effect of stress shielding.

5.4 Preliminary Results of Validation

The prototype together with the implant was mounted on the material testing machine (Instron, United States) for compression test. Due to difficultly in controlling mounting and applied force, manual load application mode was preceded. **Fig. V-11** shows the stress contour of different load application. The relative position of the contour to the tibial insert was arbitrary.

Fig. V-11 Pressure contour of Fuji film at 58.64N (left), 78.25N (center), 102.60N (right) compressive force.

The stress contour of about 50N compressive force showed less stress pattern on the film, while that of about 100N showed both pressure patterns on the bicondylar regions. All of the results showed maximum contact stress at the medial condyle region posteriorly. The color density values were 1.21, 1.45 and 1.48. However, all these values in curve C exceeded the permissible error range. The contact pressure of compressive force would have about 12MPa contact stress. The latter two exceeded the measurable range this Fuji film. About 14MPa and 15MPa would be found by interpolating the calibration curve.

The scaled simulation of the FEA was based on the setting of the experiment validation. The material used by the prototype bone was ABS P400, with strength modulus of 1834MPa and Poisson's ratio of 0.34. Compressive load of 58.64N, 78.25N and 102.60N, as the experiment was applied to the model. The predicted results of the contact pressure of tibial insert were presented in **Fig. V-12**.

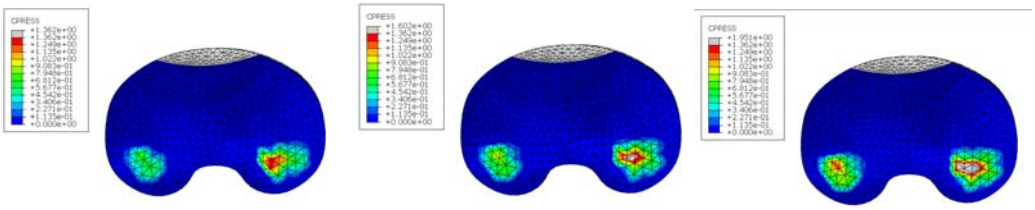

Fig. V-12 Predicted FE results at compressive load of (left) 58.64N, (center) 78.25N and (right) 102.60N.

The predicted peak contact pressures were 1.362MPa, 1.602MPa and 1.951MPa, which was apparently smaller than that of experimental results. All of the predicted stress distributions were of area contact. The Fuji film results had relative less contact area, compared with FE prediction or other pressure-sensing experiment; this could due to the hardness of the Fuji film difficult to be confined into the curved contour of the implant, leading to wrinkles inside. K-Scan (Tekscan Inc., USA) could be imported for the experiment for better contouring on the implant, as well as calibration of the device. The alignment of the implant was difficult to maintain, due to the special geometry of the bones. Rotations of the bones were difficult to resist. A special fixation had to be made to keep the bones in place, especially in validation experiment of studying the effect of flexion.

5.5 Limitations of this study

The implant model used in the study is a specific model. The predicted FE results may only specific to the current implant design. As new design concepts were coming out, new implants may have more special features, for example,

demonstrating real kinematics, deep flexion, or for high-activity use. Individual designs also gave different contact area, stress at different loading and flexion angle (Bristo et al., 1994). Some of the conditions, such as displacement input or load input may not be applicable to these design features. The knee model had only included the bones of tibial and femur, the robust of other soft tissues had not taken into account. Some constraints, such as ligaments and muscles or soft tissue impingement could affect the result outcome.

Since implant manufacturers would not disclose their implant designs, the model of implants were captured by reverse engineering technique. However, the scanned model captured was of point cloud format. The parametric information was based on the technical and clinical knowledge to build the model by the volume of point cloud. Implant manufacturers may have their parametric designs based on their criteria. Using these criteria to construct a computational model could be more accurate and could facilitate better parametric study based on varying targeted design features. In fact, the reverse engineering technique consists of error contributed from optical resolution/accuracy, as well as the optimization upon noise reduction via software.

The alignment and surgical resection was based on mathematical analysis of the model. In real situation, clinicians had to assess individual patients' limb alignment and pathology to determine the best surgical planning. Alignment and surgical deviation could be large and affect the implant performance.

In the simulation of gait walking, the boundary condition given by the ISO is universal for implant testing. In fact, as patient's knee could adapt to new walking gait, knee implant designs may not always expect to produce the same knee kinematics. For example, anatomical implant designs mimic real knee kinematics. However, functional implant design may focus on producing simple joint axis and reduce implant wear or allow high demand of activity. Using a fixed kinematic data as the boundary condition to simulate gait would over-constrain the components and lead to additional stress. In fact, values larger than three times body weight was reported (Costigan et al., 2002; Kuster et al., 1997). Maximum load could reach to 6 times body weight (Seireg & Arvikar, 1975). Heinlein et al. (2009) also believed that the boundary condition of the ISO-14243-1 was not strict enough and higher torque should be imposed.

The data acquisition via MRI imposed certain errors, such as machine error and

software segmentation error, despite the fact that the outcome of model construction via clinical imaging is relatively accurate. MRI with a registration on CT scan could yield better image quality for segmentation of different portion, such as bone, soft tissue and ligaments. However, due to the ethical guidelines in research in Hong Kong, there is a tight regulation in applying CT scan because of its radiation hazard. Meanwhile, MRI was applied as the most convenient and appropriate option.

In carrying out FE simulations in this study, some simplifications and assumptions had been imposed. In terms of material properties, the cortical bone was assumed orthotropic and the trabecular bone was isotropic. Both of the stiffness of the bone was assumed homogeneous. In carrying out the parametric study, due to the relative rigidity of cortical bone, the stiffness of cortical bone was kept constant and only the stiffness of trabecular bone was changed. The material properties of titanium alloy and UHMWPE used in the model were adopted from existing literature, whereas different manufacturers could use different types of the material. Material test on compressive strength and strain should be done to confirm the material properties of titanium alloy and UHMWPE. Parametric study of these materials could also be preceded. In fact, Au et al. (2007) commented that changing of material property of implant would influence the stress distribution and magnitude of the bone, because stiffer material take over much of the bone stresses. Villa et al. (2004) investigated the UHMWPE with fourth-order constitutive relationship. Gefen (2002) suggested that orthopaedic fixation with elastic properties of natural bone would reduce the effect of stress shielding.

In load and boundary conditions, the interface between the bone and implant were assumed to be hard contact with a coefficient of friction. In fact, a filler layer of cement should be formed between the interfaces. Moreover, some of the surface of the implant was coated with beads which encourage ingrowth of bone tissues. The interface interaction of embedded tissues could vary with time makes it difficult to be simulated in the FEA. The alignment and surgical resection of the bone to implant was based on mathematical analysis of volume and shape, whereas in real situation, a clinician would assess the patient's lower limb environment and the pathology of the knee joint to determine the alignment and resection, of which could impose large deviations.

The FE results lack concrete validations to backup. Existing FE results may produce a reference but is not strictly comparable due to their specific implant

model and different FE settings. The discovery from the current FE results also requires further clinical observations to support the hypothesis.

CHAPTER VI CONCLUSIONS AND FURTHER STUDY

6.1 Conclusions

TKA has been a common option to treat knee pain. Computational methods provide an efficient and object approach to investigate different parametric effect. In this research, a computational platform by using FEA was developed. Previous FEA often focused on contact pressure of tibial insert. In fact, FEA comprised of bone-implant complex could be helpful in understanding the influence of implant on the bones.

The sensitivity of load and flexion angle was assessed on the contact pressure of tibia insert, followed by the simulation of gait condition. This study could compare the result with existing literatures. Contact pressure was sensitive to the magnitude of load and less sensitive to flexion angle and bone stiffness. Under 2000N compressive force, the predicted minimum contact stress was 23.389MPa at 30-degree, while the predicted maximum contact stress was 25.68MPa at 60-degree. The result was comparable to existing literatures and fall within the yielding of tibial insert material.

The parametric study of bone stiffness could investigate its influence on periprosthetic fracture. Von Mises stress, principal shear and strain were presented. With BMAD less than 0.02, the von Mises stress of trabecular femur reached to about 1.5MPa; principal shear reached to about 0.5MPa; strain reached to about 0.2% at neutral position. BMAD less than 0.02 could lead to high stress, shear and strain in the FE prediction, which exceeded the yielding of bone and lead to possible risk of fracture.

The ratio of von Mises stress at the bone-implant interface was defined as stress transfer parameter (STP). The STP was about 6% at BMAD of 0.01 and reached to about 10% at BMAD of 0.1. Stress sharing of the bone was about 6-10%, corresponding to 80% stress reduction of bone in Completo et al. study (2009).

Current studies process much significance in the area. First of all, The computational platform for TKA had contained both section of femur and tibia as well as all implant components, except patella, of which comparative more comprehensive than existing models. The cortical bone was applied with a more

realistic orthotropic material properties, while the sensitivity of trabecular bone, differently, in the trabecular tibia and femur, were studied. Secondly, The FE model had been applied to study scenario and clinical situations, such as periprosthetic fracture and stress shielding. The investigation on the relationship between bone density and risk of fracture provided quantitative information about periprosthetic fracture to clinicians that have not been previously reported. Lastly, current study made use of a prototype-feedback approach to validate the FE model via Fuji film, since the validation of knee implant is difficult due to knee's sophisticated kinematics and ethical issues. Though the approach was not well-established, the inspiration could be continued to validate knee implant model invasively.

This research aimed to provide a design platform in aiding the design and manufacturing of knee implant. Parametric approach could demonstrate the capability of the platform and aid engineers and clinicians in understanding the mechanism of knee implant and knee. The parametric study in this research demonstrated the understanding of the relationship between bone density and periprosthetic fracture and stress shielding.

6.2 Suggestions for Further Study

In this study, parametric study on loading, knee flexion angle and bone stiffness has been carried out and verified with existing literatures and clinical findings. In fact, other parameters could be considered to establish more comprehensive environmental factor considerations, aid in implant design or establish treatment protocols. Coefficient of friction, bone-implant interactions could be studied to understand their effects on stress distribution on bones and implants. Surgical deviation, such as malalignment of implant alignment, subject-specific knee alignment, could be studied to aid in establish more precious surgical guidelines. Parametric study on different knee implant features, such as ML/AP ratio, stem length, flange size, could be benefit to allow optimization of knee implant design and mass-customization of implant size and geometry.

No matter FE studies, or experimental studies, research results only focus on specific knee implant design models and make results incomparable. Standard testing protocol should be established to unify the methodology or FE study and experimental study. Different implant designs should be characterized in terms of their parametric features, such as curve surface radius, implant length/width and stem length.

The boundary condition provided by ISO-14243-3 may not be universal to all implant designs, because different implant designs may design different locus of knee movement that not necessary to be inappropriate. The standard should be at least categorized into anatomical design and functional design. In fact, the ISO standard was designed for testing of implant, of which the bones were not considered. As a result, current simulation imposed assumption on the application of the boundary conditions on the bone instead of the implant. Heinlein et al. (2009) commented that applying conditions by nomenclature of knee joint was not appropriate. Force and moment components on the implant should be studied for better boundary input. Heinlein and his colleague (2009) developed an instrumented telemetric tibial tray (**Fig. VI-1**) to study the forces and moments of the implant, while level walking, stair-climbing and stair-descending, aiming to provide continuous kinematic assessment in-vivo. These data would be useful in establishing accurate boundary conditions for FEA.

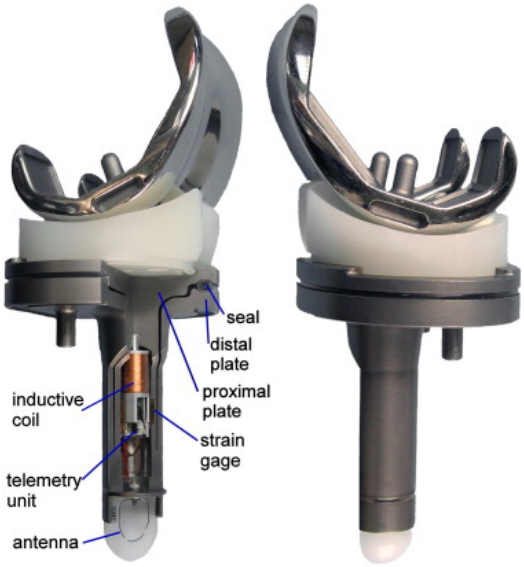

Fig. VI-1 Instrumented tibial tray developed by Heinlein et al. (2009) to study the forces and moments of the implant.

Since controlled kinematic data were input to the FEA, the effect of malalignment of implant components or individual subject knee alignment had not carefully taken into considerations, because the knee could alert the kinematics to adapt the malaligned implant. A knee-ankle-foot complex FE model, embedded with the implant model, should be developed. Together with the motion capture system and force platform, the adaption of the lower extremity could be assessed and the boundary conditions applied on the model should be more accurate. The model could also study gait alteration by different implant designs as well as surgical deviations. A more detailed anatomical model including soft tissues and ligaments

could also monitor the kinematic role of ligament as well as soft tissue impingement effects of the implant.

Further clinical application could be studied, such as effect of misalignment, cementing and mismatch, while the current model could also further extend to study different design parameters on the clinical outcome.

REFERENCES

ABAQUS theory and user's manual, version 6.7, 2007. Hibbitt, Karlsson and Sorensen Inc., Pawtucket, RI, USA.

Agency for Healthcare Research and Quality (AHRQ), Hospital Stays 15. Kaiser Family Foundation, "Range of Medicare Payments."

Ashman R.B., Cowin S.C., van Buskirk W.C., 1984. A continuous wave technique for the measurement of the elastic properties of cortical bone. J. Biomech. 17, 349-61.

Au A.G., Raso V.J., Liggins A.B., Amirfazli A., 2007. Contribution of loading conditions and material properties to stress shielding near the tibial component of total knee replacement. J. Biomech. 40, 1410-6.

Bartel D.L., Bicknell V.L., Wright T.M., 1986. Effect of conformity, thickness, and material on stresses in ultra-high molecular weight components for total joint replacement. J. Bone Joint Surg. Am. 68, 1041-51.

Beillas P., Papaioannou G., Tashman S., Yang K.H., 2004. A new method to investigate in vivo knee behavior using a finite element model of the lower limb. J. Biomech. 37, 1019-30.

Bremner J.M., Lawrence J.S., Miall W.E., 1968. Degenerative joint disease in a Jamaican rural population. Annals of the Rheumatic Diseases 27(4), 326-332.

Bristol R.E., Fitzpatrick D.C., Brown T.D., Callaghan J.J., 1994. Non-uniformity of contactstress on polyethylene inserts in total knee arthroplasty. Clin. Biomech. 11, 75-80.

Cameron H. and Cameron G., 1987. Stress-relief osteoporosis of the anterior femoral condyles in total knee replacement: A study of 185 patients. Orthop. Rev. 16, 449-56.

Carmona L., 2000. The prevalence of 6 rheumatic disease in the Spanish population. Annals of the Rheumatic Diseases.

Carr B.C. and Goswami T., 2009. Knee implants - Review of models and biomechanics. Materials and Design 30(2), 398-413.

Chiu K.Y., Zhang S.D., Zhang G.H., 2000. Posterior slope of tibial plateau in Chinese. J. Arthroplasty 15, 224-7.

Chu T, 1999. An investigation on contact stresses of New Jersey Low Contact Stress (NJLCS) knee using finite element method. J. Sys. Integr. 9, 187-99.

Ciarelli M.J., Goldstein S.A., Kuhn J.L., Cody D.D., Brown M.B., 1991. Evaluation of orthogonal mechanical properties and density of human trabecular bone from the major metaphyseal regions with materials testing and computed tomography. J. Orthop, Res. 9, 674-682.

Completo A., Talaia P., Fonseca F., Simoes J.A., 2009. Relationship of design features of stemmed tibial knee prosthesis with stress shielding and end-of-stem pain. Material and Design 30, 1391-7.

Costigan P.A., Deluzio K.J., Wyss U.P., 2002. Knee and hip kinetics during normal stair climbing. Gait Posture 16, 31-7.

Croft P., Coggon D., Cruddas M., Cooper C., 1992. Osteoarthritis of the hip: an occupational disease in farmers. British Medical Journal 304, 1269-1272.

David L.K., Tony M.K., 1998. Yield strain behavior of trabecular bone. J. Biomech. 31, 601-8.

Davis M.A., Ettinger W.H., Neuhaus J.M., Hauck W.W., 1988. Sex differences in osteoarthritis of the knee. The role of obesity. American Journal of Epidemiology 127(5), 1019-1030.

DelValle M.E., Harvin S.F., Maestro A., Murcia A., Vega J.A., 1998. Immunohistochemical analysis of mechanoreceptors in the human posterior cruciate ligament: a demonstration of its proprioceptive role and clinical relevance, J. Arthroplasty 13(8), 916-922.

Dammak M., Shirazi-Adl A., Schwartz J., Gustavson L., 1997. Friction properties at the bone-metal interface: Comparison of four different porous metal surfaces.

J. Biomed. Mater. Res. 35, 329-36.
Deborah S., Colin M., Bruce P., 2000. Global burden of osteoarthritis in the year 2000. World Health Organization Health Information and Statistics. http://www.who.int/en/ (accessed 6 July 2010)
Douglas A.D., 2001. Periprosthetic fractures following total knee arthroplasty. J. Bone Joint Surg. Am. 83A, 120-30.
Edward T.S., Hargovind D. and Paul E.D.C., 2004. Periprosthetic femoral fractures above total knee replacement. J. Am. Acad. Orthop. Surg. 12, 12-20.
Fernadez J.W. and Hunter P.J., 2005. An anatomically based patient-specific finite element model of patella articulation: towards a diagnostic tool. Biomechan. Model Mechanbiol. 4,20-38.
Gefen A., 2002. Computational simulations of stress shielding and bone resorption and around existing and computer-designed orthopaedic screws. Medical and Biological Engineering and Computing 40, 311-22.
Georgeanu V., Gruionu L., 2006. Correlation between joint kinematics and polyethylene wear using finite element method for total knee replacement. Medica 1, 38-42.
Gibson T., Hameed K., Kadir M., Sultana S., Fatima Z., Syed A., 1996. Knee pain amongst the poor and affluent in Pakistan. British Journal of Rheumatology 35(2), 146-149.
Godest A.C., Beaugonin M., Haug E., Taylor M., Gregson P.J., 2002. Simulation of a knee joint replacement during a gait cycle using explicit finite element analysis. J. Biomech. 35, 267-75.
Green G.A., 2001. Understanding NSAIDS: from Aspirin to COX-2, Clin. Cornerstone 3, 50-59.
Han H.S., Oh K.W., Kang S.B., 2009. Retrograde intramedullary nailing for periprosthetic supracondylar fractures of the femur after total knee arthroplasty, Clinics in Orthopedic Surgery 1:201-206.
Halloran J.P., Patrella A.J., Rullkoetter P.J., 2005. Explicit finite element modeling of total knee replacement mechanics. J. Biomech. 38, 323-31
Haut Donahue TL., Hull M.L., Rashid M.M., Jacobs C.R., 2002. A finite element model of the human knee joint for the study of tibio-femoral contact. J Biomech. Eng. 124, 273-80.
Heinlein B., Kutzner I., Graichen F., Bender A., Rolmann A., Halder .M., Beier A., Bergmann G., 2009. ESB clinical biomechanics award 2008: Complete data of total knee replacement loading for level walking and stair climbing measured in vivo with a follow-up of 6-10 months. Clin. Biomech. 24, 315-26.
Hitt et al., 2003. Anthropometric measurements of the human knee: Correlation to the sizing of current knee arthroplasty systems. J. Bone and Joint Surg. Am. 85, 115-122.
Ho W.P., Cheng C.K., Liau J.J., 2006. Morphometrical measurements of resected surface of femurs in Chinese knees: Correlation to the sizing of current femoral implants, The Knee 13, 12-14.
Hoaglund F.T., Yau A.C., Wong W.L., 1973. Osteoarthritis of the hip and other joints in southern Chinese in Hong Kong. J. Bone Joint Surg. Am. 55(3), 545-557.
ISO, 2004. Implants for surgery - wear of total knee joint prostheses Part 3. Loading and displacement parameters for wear-testing machines with displacement control and corresponding environmental conditions for test.
John B., 2001. Acrylic Cement is the Method of Choice for Fixation of Total Knee implants (CON), Controversies in Total Knee Replacement. Oxford University Press.
Jones L., Hungerford D., 1987. Cement Disease, Clinical Orthopaedics and Related Research 225, 192-203.
Kellgren J.H., Lawrence J.S., 1952. Rheumatism in Coal Miners II: XRay Study. British Journal of Indepemdent Medicine 9, 197-207.
Khoo L.P., Goh J.C.H., Chow S.L., 1993. Parametric Modelling of a Knee Joint

Prosthesis. Proc. of Inst. Mech. Engrs. [H] 207(2), 115-20.
Kim Y.H., Kwon O.S., Kim K., 2008. Analysis of biomechanical effect of stem-end design in revision TKA using digital korean model. Clin. Biomech. 23, 853-858.
Kuster M.S., Wood G.A., Stachowiak G.W., Gachter A., 1997. Joint load considerations in total knee replacement. J. Bone Joint Surg. Br. 79, 109-13.
Liau J.J., Hu C.C., Cheng C.K., Huang C.H., Lo W.H., 2001. The influence of inserting a Fuji pressure sensitive film between the tibiofemoral joint of knee prosthesis on actual contact characteristics. Clin. Biomech. 16, 160-6.
Liau J.J., Cheng C.K., Huang C.H., Lo W.H., 2002. Effect of Fuji pressure sensitive film on actual contact characteristics of artificial tibiofemoral joint. Clin. Biomech. 17, 698-704.
Liau J.J., Cheng C.K., Huang C.H., Lo W.H., 2002. The effect of malalignment on stresses in polyethylene component of total knee prostheses - a finite element analysis. Clin. Biomech. 17, 140-6.
Linde F., Hvid I. and Pongsoipetch B., 1989. Energy absorptive properties of human trabecular bone specimens during axial compression. J. Orthop. Res. 7, 432-439.
Liow R.Y.L. and Murray D.W., 1997. Which Primary Total Knee Replacement?. Ann. R. Coll Surg. Engl. 9,335-450.
Mintzer C.M. and Robertsen P.D., Rackemann S. Ewald F.C., Scott R.D., Spector M., 1990. Bone loss in the distal anterior femur after total knee arthroplasty. Clin. Orthop. 260,135-43.
Miyoshi S., Takahashi T., Ohtani M., Yamamoto H., Kameyama K., 2002. Analysis of the shape of the tibial tray in total knee arthroplasty using a three dimension finite element model. Clin. Biomech. 17, 521-5.
Murray C.J.L., Lopez A.D., Mathers C.D., Stein C., 2001. The global burden of disease 2000 project: aims, methods and data sources. GPE discussion paper No. 36. Geneva: WHO.
Murray C.J.L., Lopez A.D., 1997. Mortality by cause for eight regions of the world: Global burden of disease study.
Nagamine R., Miura H., Bravo C.V., Urabe K., Matsuda S., Miyanishi K., Hirata G., Iwamoto Y., 2000. Anatomic variations should be considered in total knee arthroplasty. J. Orthop. Sci. 2000, 5, 32-7.
Natalia A.W., Eugene S.S., Kathleen M, Kevin J.B., 2008. Hip and knee implants: current trends and policy considerations, Health Affairs 27(6):1587-98.
NHANES I: Basic data on arthritis: knees, hip and sacro-iliac joints. Adults ages 25-74 years. United States 1971-1975. U.S. Department of Health, Education and Welfare.
OrthopedicNetworkNews, 2008. Hip and knee implant list prices rise 6.3 percent, OrthopedicNetworkNews 19, 1–9.
Partridge R.E.H., Duthie J.J.R., 1968. Rheumatism in dockers and civil servants: a comparison of heavy manual and sedentary workers. Annals of the rheumatic Diseases 27, 559-568.
Penrose J.M.T., Holt G.M., Beaugonin M. and Hose D.R., 2001, Development of an accurate three-dimensional finite element knee model, Comput. Meth. Biomech. Biomed. Eng., 5(4), 291-300.
Rankin E.A., Alarcon G.S., Chang R.W., Cooney L.M., Costley L.S., Delitto A., Deyo R.A., Donaldson S.K., Hochberg M.C., Maclean C.H., Yelin E.H., Marciel K., 2004. NIH Consense Statement on Total Knee Replacement December 8-10 2003. J. Bone Joint Surg. Am. 86, 1328-1335.
Reilly D.T. and Burstein A.H., 1975. The elastic and ultimate properties of compact bone tissue. J. Biomech. 8, 393-405.
Rohlmann A., Zilch H., Bergman G., Kolbel R., 1980. Material properties of femoral cancellous bone in axial loading. Part I: Time independent properties. Arch Orthop. Trauma Surg. 97, 95-102.
Sandeep M., Kenneth A.K., 2001. The posterior cruciate ligament should routinely be salvaged during total knee replacement (PRO), controversies in total knee

replacement, Oxford University Press.
Scott D., Hofmann A., Thach T., Camargo M., Evanich C., 1997. A seven to eleven year experience with cementless fixation using the natural knee, Proceedings of the 64th Annual Meeting of the American Academy of Orthopaedic Surgeons 353.
Seirg A. and Arvikar R.J., 1975. The prediction of muscular load sharing and joint forces in the lower extremities during walking. J. Biomech. 8, 89-102.
Shuichi M., White S.E., Williams V.G., McCarthy D.S., Whiteside L.A., 1998. Contact stress analysis in meniscal bearing total knee arthroplasty. J. Arthroplasty 13, 699-706.
Solomon L., Beighton P., Lawrence J.S., 1975. Rheumatic disorders in the South African Negro. Part II. Osteo-arthrosis. South African Medical Journal 49(42), 737-1740.
Song Y., Debski R.E., Musahl V., Thomas M., Woo S.L.-V., 2004. A three-dimensional finite element model of the human anterior cruciate ligament: a computational analysis with experimental validation. J. Biomech. 37, 383-90.
Steven B.H., Khalin J.S., The posterior cruciate ligament should routinely be salvaged during total knee replacement (CON), controversies in total knee replacement, 2001, Oxford University Press.
Sun M.J., Wang H.L., Zhang Y., Wang Y.H., Wang Y., Jiang X.H., Liu L., 2002. The geometry and measurements of parameters of normal knees in Chinese, 313 Hospital of PLA 27(12), 1050-2.
Tamaki M., Koga Y., 1994. Osteoarthritis of the knee joint: a field study. Nippon Seikeigeka Gakkai Zasshi - Journal of the Japanese Orthopaedic Association 68(9), 37-750.
Thomas P.S., 1991. The painful total knee replacement, Total knee replacement, 195-198.
Tissakht M., Ahmed A.M. and Chan K.C., 1996. Calculated stress-shielding in the distal femur after total knee replacement corresponds to the reported location of bone loss. J. Orthop. Res. 14, 778-85.
Travis A.B., Jim M., Niebur G. and Ploeg H.L., 2008. Compressive properties of trabecular bone in the distal femur. J. Biomech. 1077-85.
Travis A.B., Jim M., Ploeg H.L., 2009. Initial fixation of a femoral knee component: an in vitro and finite element analysis. Int. J. Experimental and Computational Biomechanics 1, 23-43.
Tzonchev VT., 1968. Prevalence of osteoarthrisits in Bulgaria. In: Bennett PH, Wood PHN,editors. Population studies in the rheumatic diseases. Excerpta Medica, 413-415
U.S. Securities and Exchange Commission, Form 10-K, “Zimmer Holdings, Inc.,” filed 11 March 2005,http://www.secinfo.com/dsvRm.z2rd.htm#1stPage (accessed 28 April 2008); and SEC, Form 10-K,“Zimmer Holdings, Inc.,” filed 29 February 2008, http://www.secinfo.com/dsvRm.t3ZK.htm#1stPage (accessed 28 April 2008).
Valkenburg H.A., 1980. Clinical versus radiological osteoarthritis in the general population. In:Peyron JG, editor. Epidemiology of osteoarthritis. Paris: Ciba-Geigy, 53-58
Villa T., Migliavacca F., Gastaldi D., Colombo M., Pietrabissa R., 2004. Contact stresses and fatigue life in a knee prosthesis: comparison between in vitro measurements and computational simulations. J. Biomech. 37, 45-53.
Whiteside L., 1991. Effect of porous coating configuration on tibial osteolysis after total knee arthroplasty, Clin. Orthop. Res. 321, 92-97.
Woo J., Lau E., Lee P., Kwok T., Lau W.C.S., Chan C., Chiu P., Li E., Sham A., Lam D., 2004. Impact of Osteoarthritis on Quality of Life in a Hong Kong Chinese Population. The Journal of Rheumatology 12:2433-8.
Wu H.S., Wu Y.L., 2005. Artificial Knee Joint Science – From Primary to Revision Surgery, People’s Military Medical Press.